

Department of Physics and Astronomy
University of Heidelberg

Bachelor Thesis in Physics
submitted by

Alexandra Datz

born in Tübingen (Germany)

2017

Studies on Secondary Discharges and their Mitigation with a two GEM Detector

This Bachelor Thesis has been carried out by Alexandra Datz at the
GSI Helmholtzzentrum für Schwerionenforschung in Darmstadt
under the supervision of
Prof. Dr. Silvia Masciocchi

Abstract

After the Long Shutdown 2 (LS2) of the Large Hadron Collider (LHC) in 2019/2020, the interaction rate of lead-lead collisions will increase up to 50 kHz. Currently, the Time Projection Chamber (TPC) of ALICE, its main detector for tracking and identification of particles, can only handle rates up until around 3 kHz. In order to cope with the higher interaction rate, the TPC is going to be upgraded with new readout chambers, containing Gas Electron Multipliers (GEMs). However, GEMs are more prone to damages than the previously used wire chambers. A major threat are discharges, inducing a short across the foil and in the worst case causing irreparable damages. Especially discharges that occur shortly after another discharge, so called secondary discharges, carry a high risk of damaging the foil. Hence, a lot of effort is put into understanding the reason for secondary discharges and exploring possibilities for their mitigation. Some of the many parameters that have an impact on the secondary discharge probability are examined in this work. These are the foil itself and the position of the foil triggering the discharges. Moreover, this work presents a possibility to reduce secondary discharges by adding an additional resistor to the power supply path of the GEMs.

Kurzzusammenfassung

Nach dem Long Shutdown 2 (LS2) des Large Hadron Colliders (LHC) wird sich die Interaktionsrate der Blei Blei Kollisionen auf bis zu 50 kHz erhöhen. Die Time Projection Chamber (TPC) von ALICE, wichtig für die Rekonstruktion der Teilchenbahnen und die Identifikation der Teilchen, ist zur Zeit nur für Interaktionsraten von maximal 3 kHz ausgelegt. Somit wird das Upgrade der TPC mit neuen Ausleseammern notwendig. Diese werden mit Gas Electron Multiplier (GEMs) ausgestattet. Allerdings sind GEMs für mechanische Schäden anfälliger als die zuvor verwendeten Drahtkammern. Eine Bedrohung stellen vor allem die Entladungen dar, die für einen Kurzschluss der Folie sorgen und im schlimmsten Fall dauerhafte Schäden verursachen. Insbesondere sekundäre Entladungen, Entladungen die kurz nach einer anderen Entladung auftreten, haben das Potential die Folie stark zu beschädigen. Darum sind die Bemühungen groß, sowohl die Ursache als auch die Einflüsse der sekundären Entladungen herauszufinden. Diese Arbeit präsentiert verschiedene Parameter die einen Einfluss auf die Wahrscheinlichkeit der sekundären Entladungen haben. Dies sind zum einen die GEM Folien selbst, sowie die Position der Folie, welche die Entladungen auslöst. Zusätzlich zeigt diese Arbeit die Möglichkeit auf, die Wahrscheinlichkeit von sekundären Entladungen durch das Anbringen eines zusätzlichen Widerstandes zu verringern.

Contents

1. Introduction	1
2. ALICE at the LHC	3
2.1. Overview and Quark-Gluon Plasma	3
2.2. ALICE TPC and the TPC Upgrade	5
2.2.1. The TPC of ALICE	5
2.2.2. Gas Electron Multipliers (GEMs)	9
2.2.3. Discharges	13
3. Measurements	17
3.1. Setup	17
3.2. Methods	21
3.3. Results	24
3.3.1. Different GEM Foils at the same Location	24
3.3.2. Different Decoupling Resistors	27
3.3.3. Discharges triggered by GEM1	43
3.4. Discussion	46
4. Summary and Outlook	47
A. Detailed Settings of Measurements	50
List of Figures	66
References	68

1. Introduction

The "A Large Ion Collider Experiment" (ALICE) is one of four large experiments at the Large Hadron Collider (LHC) at CERN. ALICE is dedicated to studying heavy ion collisions in order to examine the quark-gluon plasma, a state of matter where the high energy density allows partons (quarks and gluons) to be deconfined. Such state of matter is assumed to have existed in the early universe, a few microseconds after the Big Bang. After the (LHC) Long Shutdown 2 (LS2) in 2019/2020 the interaction rate of lead-lead collisions provided by the LHC will increase up to 50 kHz. This imposes a challenge to the whole ALICE apparatus and, particularly relevant for this work, for the Time Projection Chamber (TPC) of ALICE since currently, it can only handle rates up to 3 kHz. This limitation is due to the gating grid which is currently needed for the optimal operation of the TPC equipped with Multiwire Proportional Chambers (MWPC). In fact, the ionization signal produced in the drift volume of the TPC is amplified in the MWPC: a gating grid is needed in order to prevent positively charged ions to move back into the drift region and therefore avoid the formation of extended space charge which would distort the drift field. However, the "closure" of the gating grid makes the TPC readout chambers blind to interactions happening in the meanwhile and therefore limits the readout rate to around 3 kHz.

To cope with the higher interaction rates after LS2, the TPC is going to be upgraded with readout chambers allowing for a continuous readout while providing a low Ion Back-Flow (IBF). The new readout chambers of the TPC will use Gas Electron Multipliers (GEMs) instead of the MWPCs. GEMs are composed of two layers of copper, separated by an insulating layer of kapton and holes through all of the three layers. If a high voltage is applied to both copper sides a high electric field is produced inside the holes in which an incoming electron can start an electron avalanche.

A single GEM has an ion back flow of around 90%, however, the IBF can be reduced to less than one percent in carefully tuned GEM stacks. It is planned to use a stack of four GEMs for the new ALICE TPC readout chambers. The ALICE TPC is going to be the first TPC operated with a continuous readout, hence a huge R&D program was started to find the proper configuration for the GEMs and the operating conditions for the whole detector.

Yet, GEMs are more vulnerable to damages than the MWPCs, which is why there is a lot of research on causes for damages of the GEMs. A major threat is the possibility of shorts in GEM foils induced by discharges. Until now there are still a lot of open questions

concerning discharge. However studies have been conducted that allow a rather detailed description of the impact they have. Usually, a discharge affects the GEM potentials, they drop or increase during a discharge. Electrical discharges can damage the foils severely or even destroy them irreparably. Once the upgraded TPC will be installed inside ALICE it is impossible to remove any of the foils and it would be a tremendous problem if a foil got damaged. Consequently, a lot of effort is put in understanding the discharges, extracting parameters that influence them and finding voltage settings at which as few discharges occur as possible.

This work is embedded in those studies. It especially focuses on so called secondary discharges. These discharges occur shortly after the primary discharge, however with a significant larger amplitude and an even greater impact on the potentials of the GEMs than the primary discharges. The research was conducted with a small detector containing a stack of two GEMs. It was examined with this detector how different parameters influence the probability, that the primary discharge is followed by a secondary discharge. One of the parameters was how different foils at the same location in the GEM stack would change the secondary probability. Additionally, the dependence of the secondary discharge probability on resistors that were added to the setup was analysed. Moreover, the occurrence of secondary discharges, while starting the discharges in the one or the other GEM was studied. In general the secondaries appear for a specific electric field, the probability of their occurrence increases rapidly with a higher field.

Secondary discharges impose, as mentioned before, a severe threat to GEM foils. Yet, their occurrence is influenced by several factors. Those described above will be described and examined within this work. A careful investigation of the exact impacts of those factors might reveal a configuration for the GEM stack that is less prone for secondary discharges and therefore safer and more stable to be operated within the TPC.

2. ALICE at the LHC

2.1. Overview and Quark-Gluon Plasma

The Large Hadron Collider (LHC) of CERN¹ is located at Geneva, Switzerland. CERN was founded in 1954, with the aim to gain more insight into the fundamental structure of the universe. Since then a lot of important discoveries have been made, among them the proof of the existence of W and Z particles, as well as the proof of the Higgs Boson. Also the world wide web was invented at CERN [1]. Moreover, crucial developments in the field of particle detectors were made at CERN, such as the multi wire proportional chamber (MWPC), invented in 1968 by G. Charpak, which he received a Nobel prize for in 1992 [2].

The A Large Ion Collider Experiment (ALICE) is one of four large experiments of the LHC. It is dedicated to heavy ion collisions in order to investigate the quark-gluon plasma (QGP), a special state of matter, in which the universe is assumed to have been just microseconds after the big bang [3].

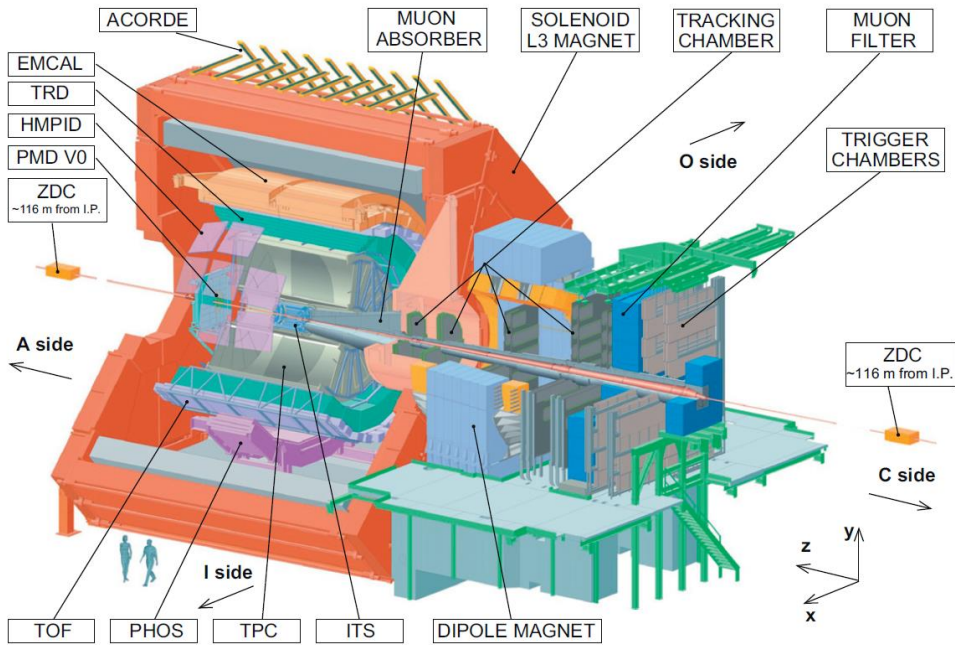


Figure 1: The ALICE detector and its subdetectors.

The ALICE detector with its subdetectors is depicted in Fig. 1. The main subdetectors from inside to outside are the inner tracking system (ITS) to localize the primary

¹ *Conseil européen pour la recherche nucléaire*- Europäische Organisation für Kernforschung

vertex and the secondary vertices, the time projection chamber (TPC), which will be explained in detail in chapter 2.2, for tracking and identifying particles, the transition radiation detector (TRD) for electron identification, the time-of-flight (TOF) detector for the identification of particles with medium momentum range, the photon multiplicity detector (PMD), the high momentum particle identification detector (HMPID) to support the identification of particles, the photon spectrometer (PHOS), the electromagnetic calorimeter to measure particles with high p_T (EMCAL) and the muon spectrometer [4], [5]. Most of the detectors lie inside the L3-magnet, which is illustrated in red in Fig. 1. Since the ALICE detector examines the QGP, the subdetectors have to cope with the high multiplicity environment produced by lead-lead collisions, which are, however, necessary to produce the QGP. The value for the charged particle multiplicity density was predicted to be $\frac{dE}{d\eta} = 1500 - 4000$. However, ALICE was even tested for $\frac{dE}{d\eta} = 8000$ [5]. Moreover the detectors are optimized for measurements of particles with a very low momentum, covering as much of the solid angle as possible. Furthermore, the detectors allow for a very precise reconstruction of the particle trajectories and their identification.

Quark-Gluon Plasma

As already described above, the universe is assumed to have been in a state of quark-gluon plasma just microseconds after the Big Bang. Consequently, it is of great interest to examine this state which might lead to more insights on the early stages of the universe and reveal new physics. QGP is a state of matter forming at a very high density and temperature. In this state quarks and gluons can move around freely, i.e. they are no longer confined. The temperature of this so called fireball is around $T = 100 - 500$ MeV which corresponds to more than 10^{12} K. For comparison, the temperature at the core of the sun is around $15 \cdot 10^6$ K, hence a million times cooler. Additionally the pressure is around $P = 100 - 300 \frac{\text{MeV}}{\text{fm}^3}$, this means 10^{35} Pa and the density around $\rho = 1 - 10 \cdot \rho_0$. However, the duration of this state is only about $3 - 6 \cdot 10^{-23}$ s.

For the formation of a QGP several stages exist:

- 1) initial collision
- 2) thermalization
- 3) expansion and cooling
- 4) chemical freeze-out
- 5) kinetic freeze-out

With hadrons being produced during stage 4 and 5 the aim is to characterize stage number 3, the fireball and the stages 1 and 2. This characterization includes the phase diagram and transport properties, as viscosity or diffusion coefficients [3].

2.2. ALICE TPC and the TPC Upgrade

2.2.1. The TPC of ALICE

The Time Projection Chamber (TPC) of ALICE is one of its main detectors for the identification and tracking of particles. With a length of 5 m, a height of 5 m and a volume of around 90 m³ it is the largest TPC in the world [6]. In the following, the layout and working principle will be described in more detail.

Layout of the TPC

As depicted in Fig. 2, the TPC is cylindrical, covering as much of the solid angle as possible around the interaction point. The volume, which is filled with a gas mixture of currently 90% Argon and 10 % Carbondioxide [7], is divided into two equal parts by the central high voltage electrode. At the two endplates the readout chambers of the TPC are located, the inner readout chambers (IROC) and outer readout chambers (OROC). They consist of multi-wire proportional chambers (MWPCs) with more than half a million readout pads [6] and a gating grid, that is installed in front of them [8]. The electric field between the central electrode and the endplates is parallel to the beam line with a strength of $400 \frac{\text{V}}{\text{cm}}$ [9], its homogeneity is ensured by two field cages, the inner and outer field cage. The field cages consist of strips attached to the walls of the TPC, which have potentials adjusted so that they match the local potential difference between the central cathode and the endplates. As mentioned before, the TPC lies inside a magnet which provides a magnetic field of maximum 0.5 T [8] that is parallel to the electric field.

Working Principle

A charged particle passing through the TPC ionizes the gas along its path. The electrons produced within this primary ionization drift towards the endplates, the ions towards the central HV electrode. At the endplates the electrons pass through the gating grid, that is installed in front of the MWPCs. This is opened when it receives a signal from the trigger, in order to record the data. After passing the gating grid, the electrons are amplified in the region around the anode wires, due to the strong electric field in

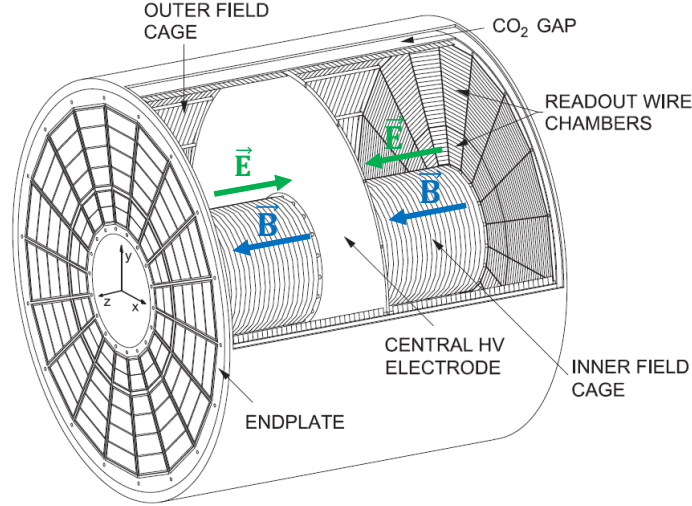


Figure 2: The TPC of ALICE. The orientations of the magnetic and electric field lines are depicted in blue and green respectively ([10], p.8).

the vicinity of the wires. The ions produced during this amplification then induce a positive signal on the pad plane. Moreover, ions are prevented from drifting into the drift volume by closing the gate after all primary electrons have passed. The closing of the gate is achieved by applying a different voltage on the wires, i.e. the potentials are alternating $U \pm \Delta U$ [8]. This closure is crucial, since ions drifting back would lead to huge space charge distortions of the drift field and would therefore complicate or even distort the readout of the signals. This is also the reason for the limitation of the TPC to a maximum interaction rate of 3 kHz. The gating grid in front of the MWPCs needs to stay closed until all ions are neutralized i.e. have travelled back to the central electrode, which takes around 200 μs . Additionally the maximum drift time of electrons inside the TPC is around 100 μs [11], consequently the limit for the interaction rate is around 3 kHz.

Information retrieved from Data

For the reconstruction of the tracks inside the TPC the drift time of the electrons provides information on the z coordinate (parallel to the beam axis) of the original trajectory, whereas the position of the signal in the readout plane gives information on the $r\phi$ - coordinate. The pad plane is segmented in 159 pad rows in radial direction. The magnetic field decreases the transversal diffusion, contributing to the fact that even after a drift length of more than two meters the position of the original particle trajectory can be reconstructed precisely. Moreover, it causes the tracks of the particles to bend, hence

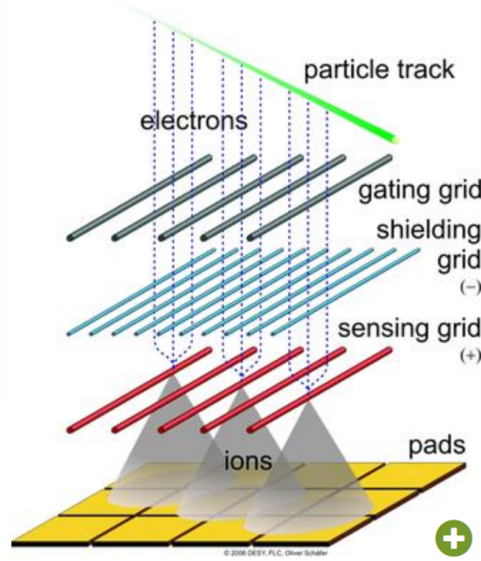


Figure 3: Drift path of electrons in the MWPCs for an open gating grid. The electrons are amplified in the vicinity of the anode wire grid (or sensing grid). The ions induce a positive signal in the pads [12].

it is possible to determine the momentum from the bending radius [13]. The information arriving at the readout plane, however, does not only contain the location of the track, but also how much energy the particle deposits along its way, since this is proportional to the primary electron ion pairs produced [14]. Consequently all this information allows for a reconstruction of the particle trajectories and additionally for their identification. The measurement by the TPC of the energy loss dE/dx as a function of the momentum p can be seen in Fig. 4. The data presented were measured during lead-lead collisions with a center of mass energy of $\sqrt{s_{NN}} = 2.76$ TeV.

This distribution is theoretically described by the Bethe - Bloch formula

$$-\left\langle \frac{dE}{dx} \right\rangle = K \frac{Z}{A} \frac{z^2}{\beta^2} \left[\frac{1}{2} \ln \frac{2m_e c^2 \beta^2 \gamma^2 T_{max}}{I^2} - \beta^2 - \frac{\delta(\beta\gamma)}{2} - \frac{C(\beta\gamma, I)}{Z} \right], \quad (1)$$

which gives the mean energy loss, usually normalized with respect to the density.

With γ being the Lorentz factor and β the velocity of the particle it becomes clear that the energy loss is dependent on the mass of the particle, since different masses cause a different β and γ for the same momenta. Hence, the specific energy loss is different for different particles [14]. This can be seen in Fig. 4, where the energy loss of the particles is clearly distinguishable. For momenta below 1 GeV the identification

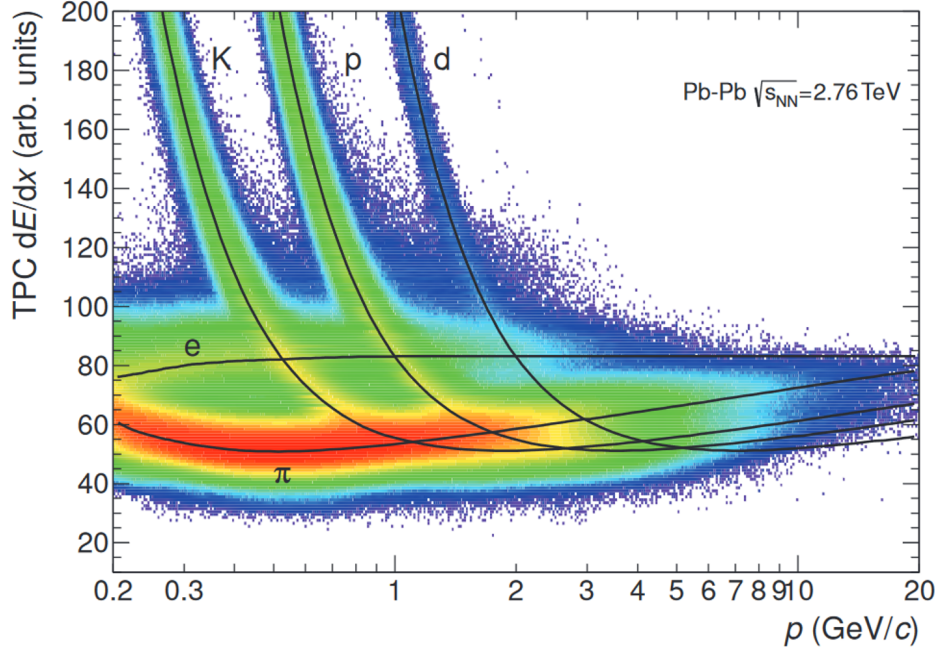


Figure 4: Specific energy loss as function of momentum p for particles from lead-lead collisions with a center of mass energy per nucleon pair of $\sqrt{s_{NN}} = 2.76$ TeV. The black lines represent the expected mean energy loss. [15]

is achieved by simply comparing the different bands retrieved from the measurements with the theoretical calculations. For higher momenta it is still possible to distinguish between the particles on a statistical basis [15].

TPC Upgrade

After the LHC Long Shutdown 2 (LS2) in 2019/2020 the interaction rate of lead-lead collisions will increase up to 50 kHz. However, the current TPC can only handle interaction rates up to about 3 kHz, as described above. This necessitates an upgrade of the detector during LS2 in order to profit from the higher interaction rate, which also means more statistics and a higher precision for the measurements [16]. For the upgrade it is planned to transform the readout of the TPC to a continuous readout. This is not possible while still employing the MWPCs, albeit with an open gating grid. The ion back flow caused by an open gate would create too large space distortions of the drift field, therefore a lot of effort was invested into finding an alternative for the readout of the TPC. This resulted in the choice for chambers equipped with Gas Electron Multipliers (GEMs), which will be explained in more detail in the next chapter.

2.2.2. Gas Electron Multipliers (GEMs)

The Gas Electron Multiplier (GEM), a special sort of Micro-Pattern Gas Detectors (MPGD), was invented in 1997 by Fabio Sauli at CERN [17]. Originally GEMs were constructed for the pre-amplification of primary electrons in front of another detector, e.g. in front of a multi-wire proportional chamber (MWPC). However today they are also widely employed as detectors themselves or as discussed here for the readout of TPCs. Currently, they are employed within several detectors such as LHCb, PHENIX, TOTEM and COMPASS, for the future they will be also utilized in ALICE and CMS ([10], p.17).

GEMs consist of three layers, two 2-5 μm thick copper layers that are separated by a third 50 μm thick insulating Kapton layer ([10], p.15). By etching the foil, which will be explained in more detail later on, a usually hexagonal pattern of holes is formed [18]. The distance between two of the holes is referred to as pitch. The standard pitch is 140 μm [10]. One of the GEMs' copper layers with holes as described above is depicted in Fig. 5. The slightly darker rings inside the holes represent the insulating layer, which can be seen due to the double- conical shape of the holes.

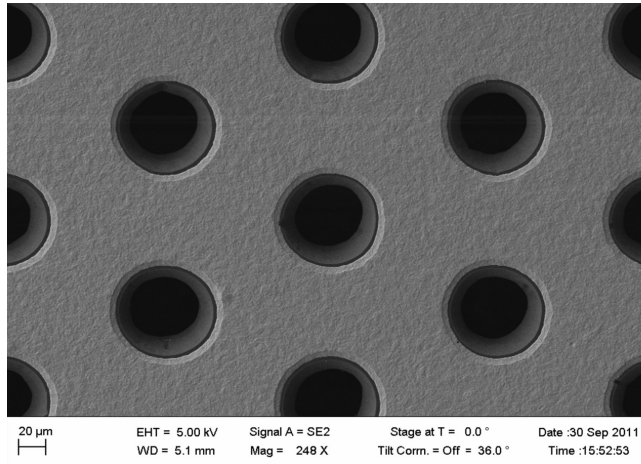


Figure 5: Electron microscope photograph of a standard GEM foil with hole pitch 140 μm ([10], p.16).

The application of a different voltage on both sides of the GEM produces a strong electric field inside the holes of $\mathcal{O}(50 \text{ kV/cm})$ ([10], p.15), which allows for electron amplification in this region. The effective gain, i.e. the gain including already losses of electrons on the GEM bottom side due to the electric field lines [20], is defined by

$$G_{eff} = \frac{I_{anode}}{eN_{ion}R} \quad (2)$$

with I_{anode} being the current measured by the readout plane, R the rate of incoming X-rays and N_{ion} the number of ionization electrons produced by each X-ray conversion. Typically, the effective gain is around $10^3 - 10^4$ for a stack of 3 - 4 GEMs ([10], p.15 ff.).

The electric field inside a hole is shown in Fig. 6. Besides depicting the electric field lines, this figure indicates that the GEM suppresses some of the ions that are produced in the region of the high field from drifting into the drift region, where the amplified electron was originating from. This intrinsic suppression is about 10 % [11], which is achieved by a combination of asymmetric field lines, that end more often on one side of the GEM for ions than for electrons and by the fact that ions follow these field lines more closely due to their smaller diffusion.

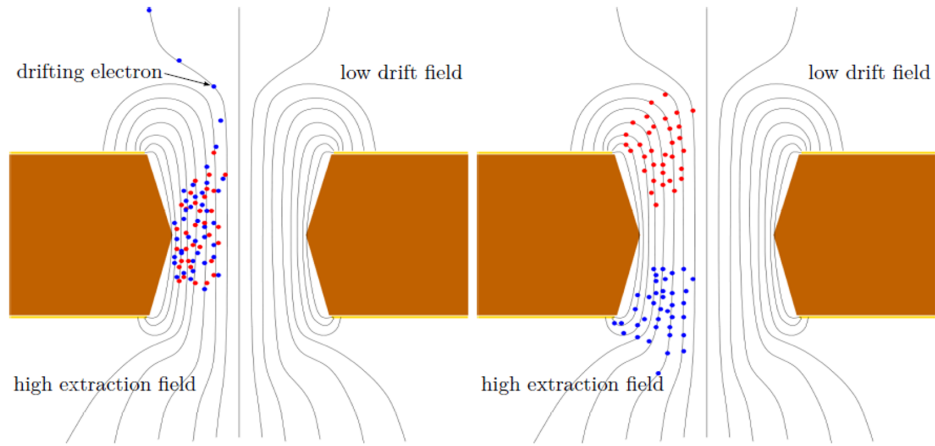


Figure 6: Electric field inside a hole of a GEM [21]. Electrons are depicted in blue and ions in red. This picture also shows the double-conical shape of the holes.

In general, according to one of several definitions in literature, the ion back flow (IBF) can be calculated as follows:

$$IBF = \frac{I_{cathode}}{I_{anode}} = \frac{1 + \epsilon}{G_{eff}} \quad (3)$$

Here, ϵ represents the number of ions produced in the amplification region that drift back in the drift volume per incoming electron ([10], p.17) and G_{eff} is the effective gain as defined in Eq. 2.2.2.

GEM Application inside the TPC

Despite the intrinsic ion back flow suppression, its value is far too low for an application in the ALICE TPC, since it would nevertheless lead to huge space charge distortions of the drift field. To resolve this problem for the upgraded TPC not one GEM is utilized, but a stack of four GEMs which is expected to keep the ion back flow below the 1% necessary for a successful operation within the TPC. Additionally, a stack of four GEMs allows for a high gain without too high voltages applied to the single GEMs. However, the energy resolution decreases for a stack that is optimized for a small ion back flow, since it is not transparent for all incoming electrons anymore. Hence, the final layout must be a compromise of a very good ion back flow suppression and a sufficient energy resolution [10]. The configuration that proved to have the best properties can be seen in Fig. 7. As mentioned before, the stack consists of four GEMs. GEM 2 and GEM 3 have a pitch of 280 μm , whereas GEM 1 and GEM 4 have a pitch of 140 μm .

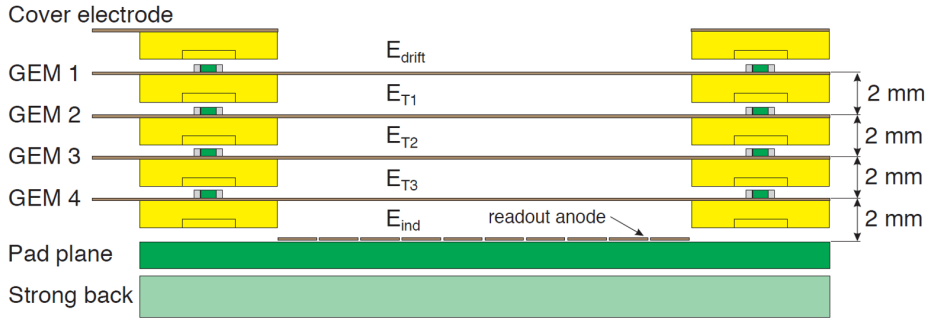


Figure 7: Stack of four GEMs as planned for the upgraded TPC ([10], p.21).

Table 1 shows the planned configuration for the voltages of the GEMs and the resulting values of the electric fields between them. For a stack of GEMs there are three differently labelled electric fields

- drift field E_D
- transfer field E_T
- induction field E_{Ind}

The drift field refers to the electric field between the drift cathode and the top side of GEM1. The transfer field for a stack of several GEMs is between adjacent foils. The induction field finally describes the field between the last GEM bottom side and the readout plane.

	Setting
ΔU_{GEM1}	270 V
ΔU_{GEM2}	250 V
ΔU_{GEM3}	270 V
ΔU_{GEM4}	340 V
Drift field	0.4 kV/cm
Transfer Field 1	4.0 kV/cm
Transfer Field 2	2.0 kV/cm
Transfer Field 3	0.1 kV/cm
Transfer Field 4	4.0 kV/cm

Table 1: Voltage configuration for the stack of four GEMs ([10], p.28).

Moreover, the top sides of the GEMs, i.e. the sides facing the drift volume, are segmented and there is a 10 M Ω resistor in the high voltage (HV) supply path. This is going to be explained in more detail in chapter 2.2.3. In Fig. 8 one of the foils for the IROC is depicted, the segments are clearly visible.

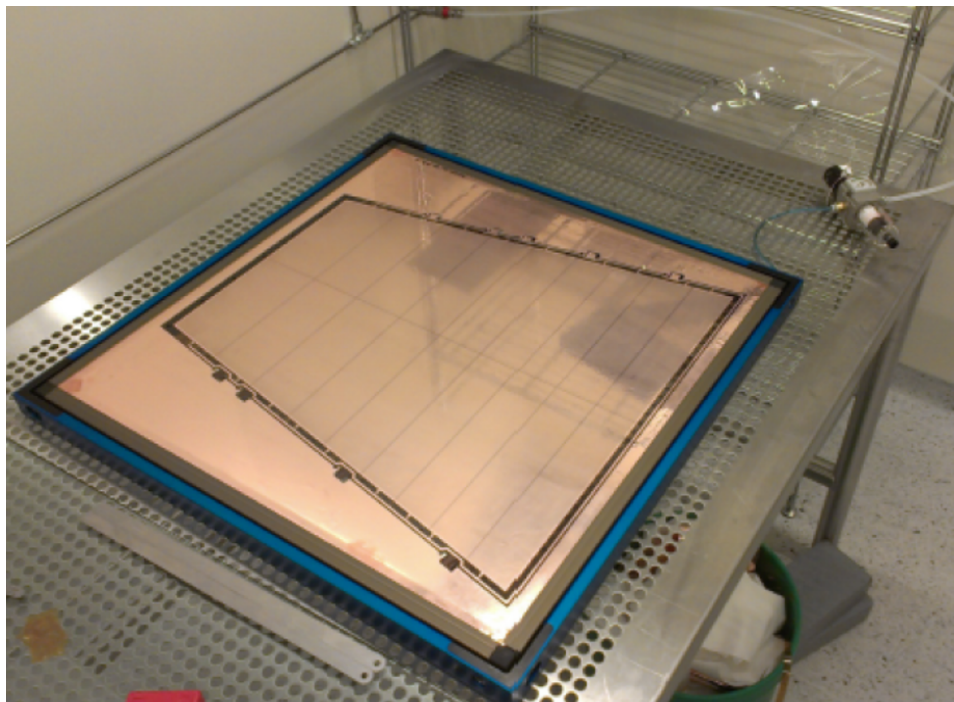


Figure 8: IROC GEM foil, before cutting and inside a stretching frame ([10], p.22).

Production of GEMs

The IROCs and OROCs of the upgraded TPC are going to contain one and three GEM stacks respectively. Although the GEM foils of the OROC cover roughly only one third of the OROCs surface, each of them is going to be large compared to commonly used GEM foils.

The double mask technique, often used for the production of GEMs, implies that two masks cover the two sides of the GEM determining the location of the holes, since the material not covered by the mask is etched away, first the metal layer then the Kapton. In order to produce GEMs of the size necessary for the OROC the double mask technique cannot be employed since it is not possible for foils that large to align the two masks on both sides of the GEM as precisely as it would be necessary. This problem is overcome by the single mask technique [19]. The main difference to the previously described technique is, as the name already suggests, that the process of etching the foils requires only one mask. This alters as well the shape of the holes, from double-conical to a quasi conical shape [20]. However, this influences the performance of the foil a bit, the gain is reduced by about 25 %, which means they have to be operated at a slightly higher voltage ([10], p.21).

2.2.3. Discharges

Primary Discharges

A major threat to GEMs are discharges. As there are still a lot of open questions on this topic, this section aims at describing the current knowledge of the impact that discharges have on GEMs and steps taken so far to prevent GEMs from discharging.

A discharge describes the effect, that in the region of the avalanche multiplication ions form a connection, a streamer, between the top and the bottom side of the GEM. This streamer then causes a spark channel. The spark causes a short across the foil which releases energy and this spark can even be seen by eye. GEMs can withstand these discharges. However when there is a lot of energy released it may cause a mechanical damage of the foil, e.g. a constant connection between the GEM top and bottom side. In case of such a damage it is not possible to apply a voltage difference which means the foil is irreparably damaged and does not contribute to electron amplification any more. To prevent the foil from being damaged through discharges several concepts were already implemented. One of them is to segment the top side, as already mentioned before. A segmentation leads to a smaller area affected by a discharge, which means a smaller amount of energy is set free since the GEM is a capacitor. Consequently, it is less

probable that a discharge will damage the foil severely. Moreover, due to the additional $10\text{ M}\Omega$ resistor in the HV supply path of the GEM top side, this potential drops on the potential of the bottom side during a discharge, as shown in studies for the ALICE TPC upgrade in [10] and in Fig. 9. So, with a segmented foil only a fraction of the GEM top side is affected, i.e. the rest of the foil remains functioning.

Furthermore, stacking the GEMs allows for an operation of each of the GEMs with lower voltage for the same gain compared to a single GEM, which also reduces the discharge probability [22].

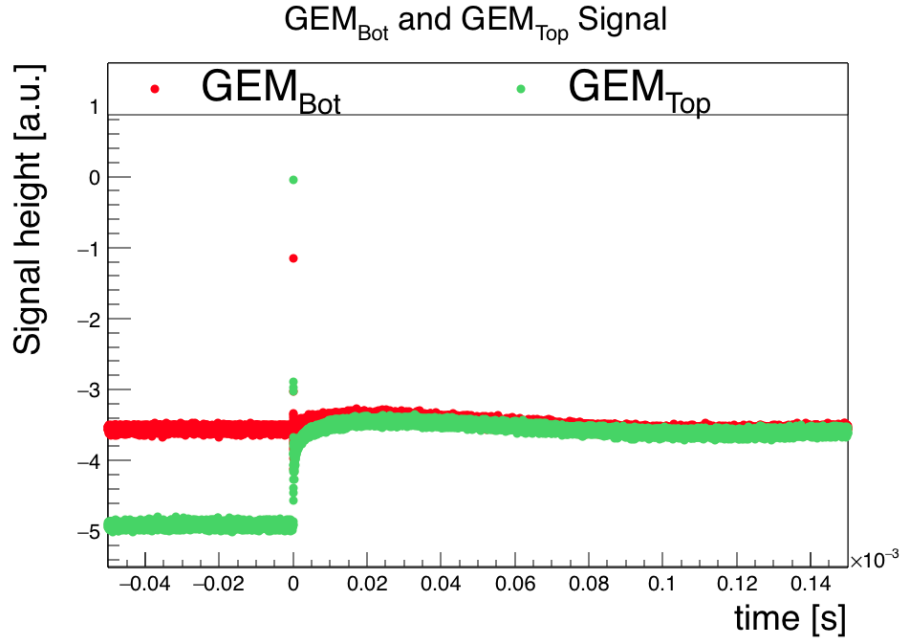


Figure 9: Potentials of a GEM during a discharge. The GEM top potential (green) drops during a discharge in this GEM on the GEM bottom potential (red) due to the $10\text{ M}\Omega$ resistor in the GEM top HV supply path [23].

Secondary Discharges

Additionally, it was observed that sometimes shortly after the first discharge a second discharge occurs [24]. This second discharge, however, changes the potentials of the GEM even more than the first, primary discharge and thus, is more prone to damage the foil. The potentials of a GEM during a secondary discharge in the induction gap can be seen in Fig. 10. Several examinations of this phenomenon revealed, that there are different parameters that influence the probability that a secondary discharge follows a primary discharge [25]. As for the primary discharges it is still not completely understood what induces secondary discharges, yet, it is crucial to understand more about them in

order to be able to safely operate the GEMs inside the TPC. A damaged foil inside the TPC would be a tremendous problem, since there is no possibility to exchange it. And without all readout chambers working there would be a gap in the readout of the TPC, hence tracking and identification of particles becomes more complicated and in the worst case would partly not be possible anymore.

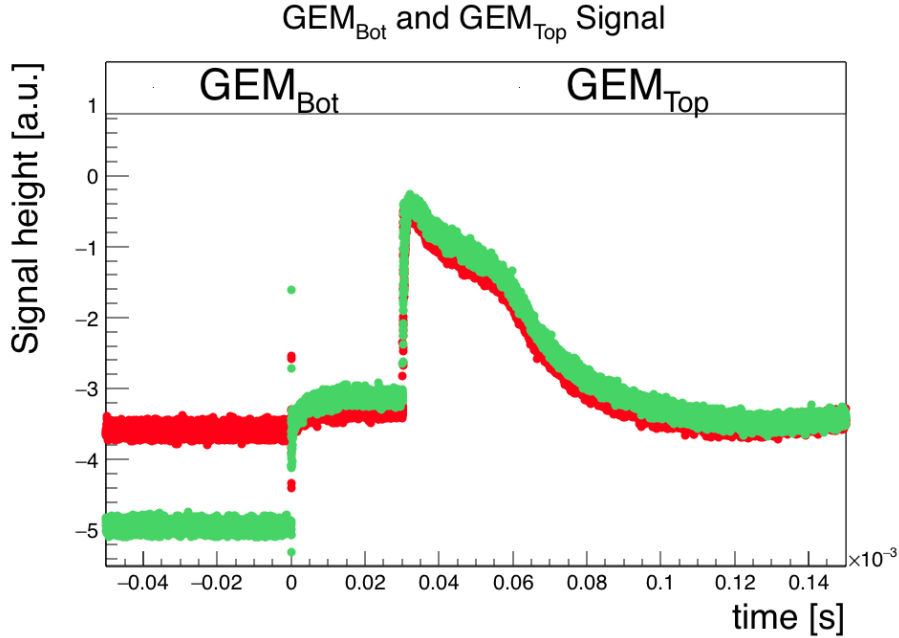


Figure 10: Potentials of a GEM during a primary discharge, followed by a secondary discharge. The GEM top potential (green) drops during a discharge in this GEM on the GEM bottom potential (red) due to the 10 M Ω resistor in the GEM top HV supply path. The secondary discharge in the induction gap causes a further drop of both potentials [23].

3. Measurements

3.1. Setup

GEM Foils

A small detector was used for the measurements, it is depicted in Fig. 11. This detector contains two $10 \times 10 \text{ cm}^2$ GEM foils, so the area is about the same as for one of the segments. Additionally, the small detector contains a drift cathode and a readout plane, this is schematically depicted in Fig. 12. The GEM foil being closer to the drift cathode is referred to as GEM1. Consequently, the other GEM is referred to as GEM2. Likewise, the part of the foil directed towards the drift volume is the top side and the other part is the bottom side of the GEM.

Electric Fields

There are three electric fields within this setup, which are described in chapter 2.2.2:

- drift field E_D
- transfer field E_T
- induction field E_{Ind}

The width of the drift gap is 30 mm while the transfer and the induction gaps are 2 mm wide, this is also indicated in Fig. 12.

Gas

The gas pressure within the detector follows the atmospheric gas pressure, since the gas system is an open one. It is composed of 90% Argon and 10% carbon dioxide, enriched with Radon, an alpha emitter, to trigger the discharges. The gas mixture of the future TPC is going to be different, Ne-CO₂-N₂ with the mixing ratio 90-10-5. Consequently the results obtained can not be easily transferred to the baseline gas mixture planned for the future TPC. This will be further discussed in chapter 3.4.

Power Supply

On the top sides of the GEM, the sides facing the drift volume, $10 \text{ M}\Omega$ resistors are mounted in the high voltage (HV) supply path similar to the configuration of the foils in the future ALICE TPC [10]. There, these $10 \text{ M}\Omega$ resistors are soldered to the segmented top sides of the GEMs. So during a discharge the top side potential will

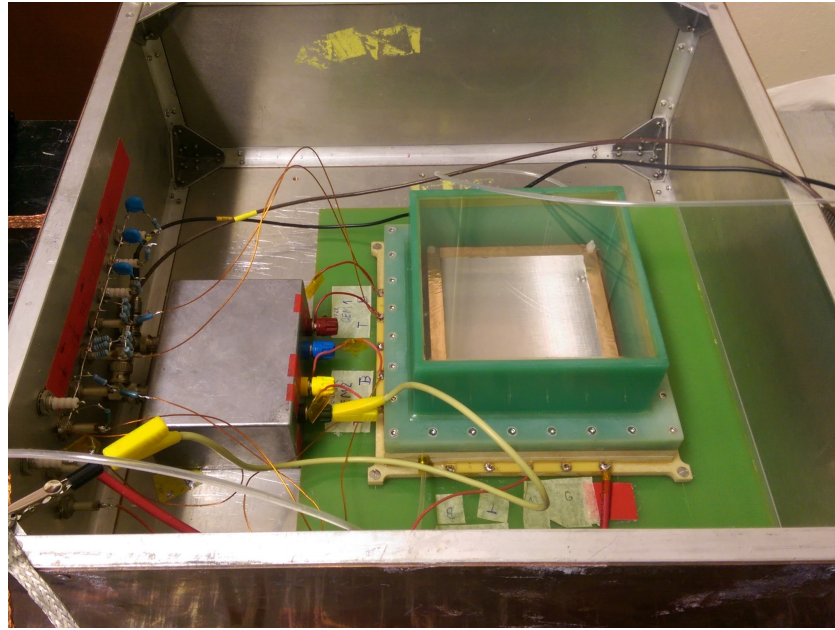


Figure 11: The setup. The green cube is the detector, the small metal box on the left contains the high voltage probes. At the left edge of the Faraday metal box the different resistors of the setup are attached to the HV feed through.

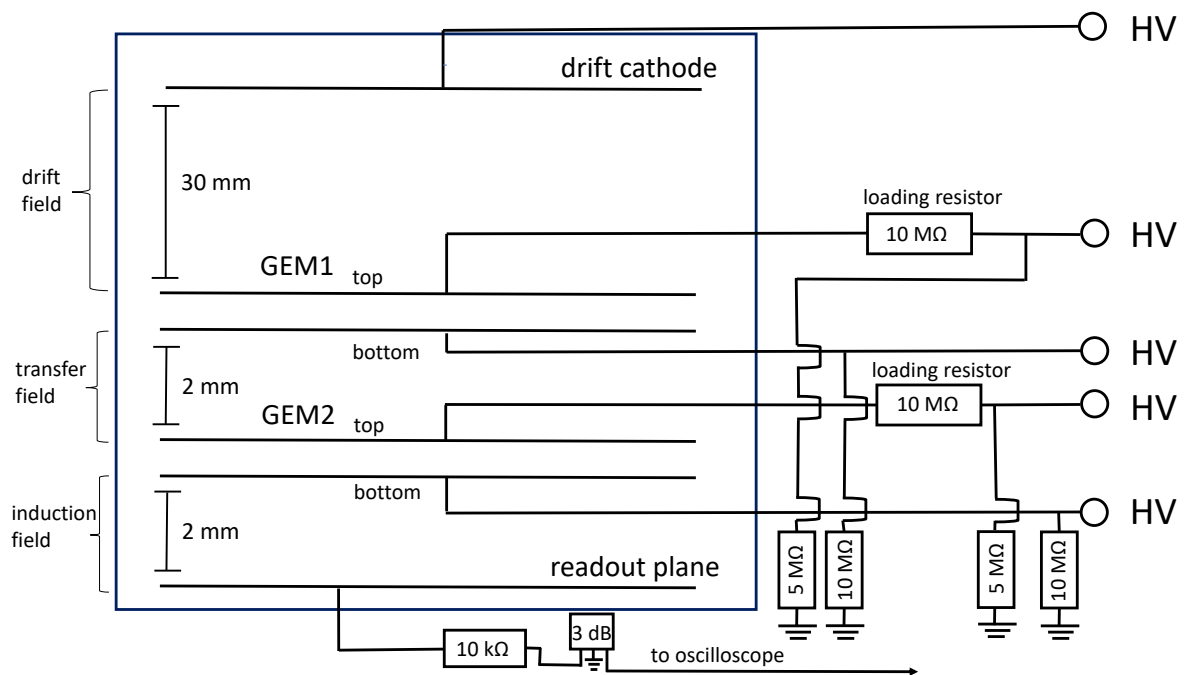


Figure 12: Schematic of the setup.

fall on the bottom side potential, i.e. most of the foil stays functioning [10]. The two resistors to ground are important for safety reasons, to make sure during a discharge i.e. a short between the foils, the current flows to ground and not directly into the high voltage power supply. The HV for the GEMs was supplied by four channels of the same power supply, so not by a cascaded power supply or a resistor chain, which were described in chapter 2.2.2. The uncertainty of the voltage supply can be estimated to be around $\pm 1V$.

Readout

The signal from the readout plane is attenuated by a 10 k Ω and 3 dB attenuator in series before reaching the oscilloscope to protect it from damage and to match the discharge signals to the dynamic range of the scope. In order to display the potentials of the GEMs on the oscilloscope as well, high voltage probes consisting of a resistor and a capacitor in parallel, were employed. In Fig. 11 the metal box in the left part of the picture contains these high voltage probes, a schematic can be seen in Fig. 13. They had to be considered during the adjustment of the voltages, since they generate additional voltage drops. However, these voltage drops only occur for the top sides, since there the 10 M Ω resistors form a voltage divider with the resistance of the the HV probe, which induces a difference between the set voltage and the voltage of the GEM. The voltage of the GEM top side U_{real} can be calculated using

$$U_{real} = U_{set} \cdot \frac{R_{os} + R_{probe}}{R_{os} + R_{probe} + R_{load}}, \quad (4)$$

which describes a voltage divider. Here, U_{set} describes the voltage of the power supply, $R_{os} = 1 \text{ M}\Omega$ is the input resistance of the oscilloscope, $R_{probe} = 345.5 \text{ M}\Omega$ the resistance of the high voltage probe and $R_{load} = 10 \text{ M}\Omega$ the resistance of the loading resistor.

Counting of Discharges

A detailed description of the counting logic that is used to distinguish between primary and secondary discharges can be found under 3.2 Methods - Logic. The number of primary and secondary discharges was counted for each of the scans, so the secondary probability could be easily calculated. A probability of 100 % for the secondary means, that for every primary discharge a secondary discharge occurs. The uncertainty of the

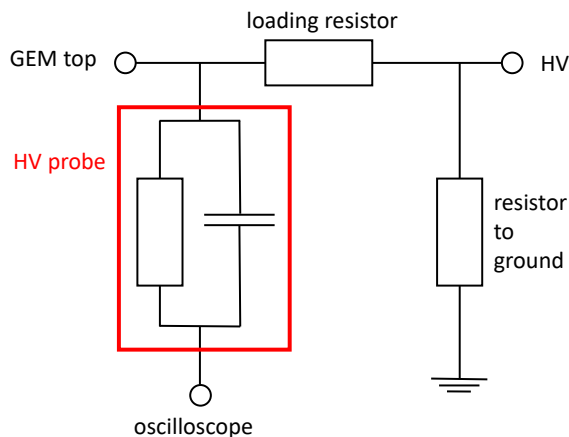


Figure 13: Schematic of HV probe position at GEM top side.

secondary probability was calculated as follows

$$\Delta \left(\frac{N_{sec}}{N_{prim}} \right) = \frac{N_{sec}}{N_{prim}} \cdot \sqrt{\frac{1}{N_{sec}^3} + \frac{1}{N_{prim}^3}}. \quad (5)$$

External Influences on the Detector

For the analysis of the data external influences on the detector have to be taken into account. One major influence is the pressure, which is permanently changing, and has an influence on the density and therefore on different properties of the gas, such as the drift velocity or the gain. Different data sets that were taken with the same electrical field but at different times are therefore difficult to compare, since density dependent parameters might have changed. Therefore, instead of the electric field itself, it is always the electric field divided by the pressure during the time of the data recording that is utilized to present results.

Moreover during all of the measurements the water to gas ratio of the detector and the temperature of the room were documented, this information can be found in Appendix A.

3.2. Methods

Procedure

The data presented in this work were obtained through different measurement series, during which one parameter was altered and the others were kept constant. This allows for studying the dependence of the secondary discharge probability on different parameters. A typical measurement consists at first of the decision on which of the two GEMs should discharge. This sets the potential difference for this GEM. The GEM discharging usually has a potential difference of $U_{GEM} = 420$ V while the other has, with some exceptions, $U_{GEM} = 260$ V. Once the voltages are decided on, the high voltage is ramped up. While ramping up it is crucial to have a small or no potential difference across the foil, to minimize the probability of discharges during the ramp up, since they could destroy the GEMs.

For a transfer field scan, the potential difference between the bottom side of GEM1 and the top side of GEM2 is increased until secondary discharges appear and even further. During a scan the potentials are increased step by step, first GEM1 bottom then GEM1 top, thus changing the transfer field, but leaving all other fields constant. During each step the numbers of primary and secondary discharges in a certain time are documented, as well as the air pressure, the water fraction in the gas mixture and the room temperature. For induction field scans, the potential of GEM2 bottom is increased, in order to keep a constant transfer field and constant GEM voltages, each of the other three potentials also have to be increased. Besides this, the procedure is the same as the one described above.

Logic

In order to count the number of primary and secondary discharges, two different counting logics were used. One distinguishes between a primary and a secondary discharge according to their peak height, the other is based on the time differences between the discharges. Of course the counting logic also has a certain dead time, however this is negligible since it is much smaller than the time between discharges, the rate for primary discharges was below 1 Hz.

For the first method, which is depicted schematically in Fig.14, the output from the readout plane of the detector was split and fed into two discriminators. Their thresholds were different, adjusted to the peak height of primary and secondary discharges respectively. The signal of each discriminator was then the input of a timing unit, providing a digital signal of adjustable length on arrival of the discriminator signal. The output

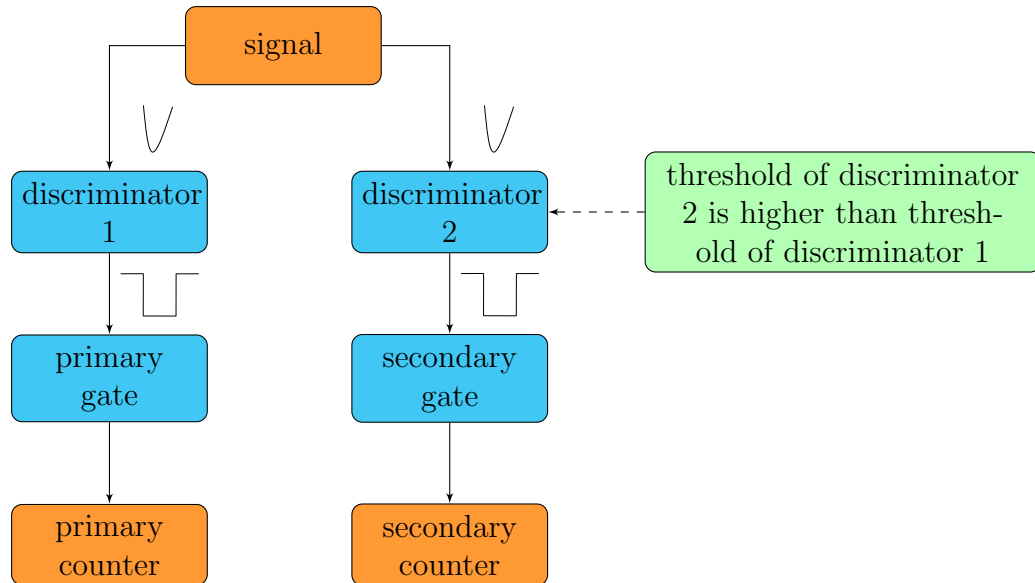


Figure 14: Counting logic that distinguishes between primary and secondary signal according to the **amplitude height**.

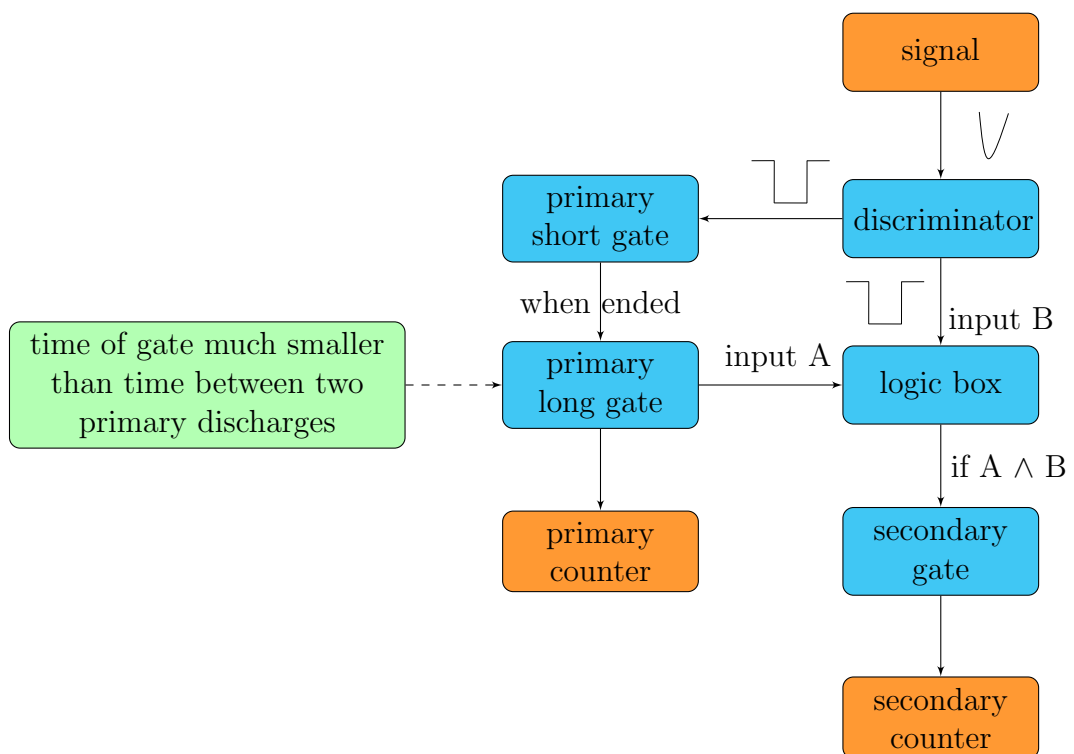


Figure 15: Counting logic that distinguishes between primary and secondary signal according to the **time difference**.

signals of the timing units were counted as primary and secondary discharges. This was necessary to prevent the primary counter from counting secondaries as primaries, since the amplitudes of secondaries also reach the threshold for primaries.

Problems with the method described above occurred when the secondary signals decreased in height, while the primary signals increased. This was e.g. the case for measurements discussed in chapter 3.3. There, the discrimination according to peak height did not work properly any more. To distinguish between the two signals it was exploited that the time difference of two primary discharges is larger than the time difference of a primary and a secondary discharge. Figure 15 shows a schematic of this method. Hence, the signal from the readout plane was only the input of one discriminator, with a threshold that primary and secondary signals would reach. This output of the discriminator was split and one part was used to trigger a timing unit, starting the 'primary short gate'. The end of the primary short gate started the so called 'primary long gate'. Each opening of this gate was on the one hand used to count the primary discharges, on the other hand it was a precondition for a signal to be counted as a secondary discharge. Only if there had been a signal, while the primary long gate was open, this signal was counted as a secondary discharge. The lengths of the different gates had to be carefully tuned to avoid missing secondary discharges or counting primary discharges as secondary discharges.

3.3. Results

To find out and understand more about the origin of primary and secondary discharges they have been studied while varying the following parameters

- the foils themselves
- additional resistors
- GEM in which discharges were triggered

To examine the influence of the foils themselves, it was studied if different foils in the same place within the same setup would cause a different discharge behaviour. Moreover additional resistors were soldered to the HV supply path of the bottom side of the GEMs and it was examined how this would influence the discharges. Additionally, it was studied how the discharges differ according to the position of the GEM, by applying higher voltages to this GEM. All of these aspects will be explained in more detail with the results obtained in the following sections. For reasons of clarity only the mean for the settings of the single measurements is presented, the detailed settings can be found in Appendix A.

3.3.1. Different GEM Foils at the same Location

One parameter that was studied was the influence of different foils at the same location on the discharges. Therefore GEM1 and GEM2 were separately exchanged. Transfer and induction field scans were conducted with both the new and the previously used GEM1, as well as for the new and the previously used GEM2.

Exchanging GEM2

In the beginning GEM2 was exchanged. In Fig. 16 the secondary probability as a function of the transfer field divided by the pressure, is shown for both the new and the previously used GEM2.

For this measurement GEM2 had a potential difference of around 420 V and the potential difference of GEM1 was around 260 V. This implies that GEM2 triggered the discharges. The induction field over the pressure was about $1.1 \frac{\text{V}}{\text{cm}\cdot\text{mbar}}$. The black stars represent the previously used GEM2 and the red stars the new GEM2. Both measurements have in common, that they show the characteristic sharp increase of the secondary probability.

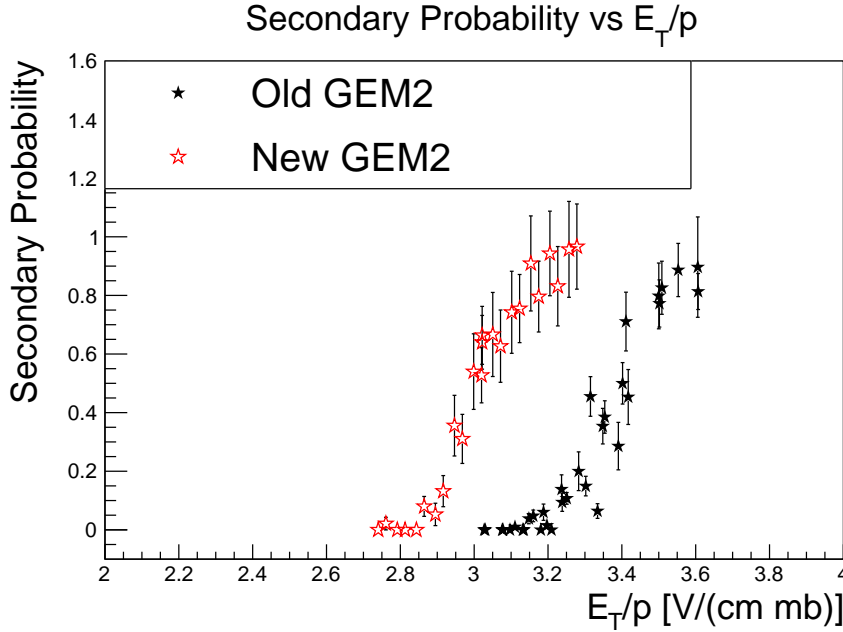


Figure 16: Comparison of secondary discharge probability of two different foils as GEM2. Discharges were triggered in GEM2. The detailed settings for the measurements can be found in Appendix A in Tab. 6 and Tab. 5.

However, they clearly differ in the onset of the secondaries. Comparing the measurements with the different foils as GEM2 reveals that the onset is shifted towards higher fields for the previously used GEM2 compared to measurements with the new GEM2. This difference is about $0.3 \frac{\text{V}}{\text{cm}\cdot\text{mbar}}$ which corresponds to approximately 58 V .

Exchanging GEM1

The same effect as described above is also observed if two different foils serving as GEM1 are compared, however still with GEM2 discharging. The relevant settings for the measurements can be found in Tab. 3.3.1. For this comparison both an induction field and a transfer field scan were conducted, the result is depicted in Fig. 17. There, the red stars indicate the old and the green stars the new GEM1. The filled symbols represent the data of the induction field scans and the empty ones that of the transfer field scans. Thus, the filled green and red stars are the comparison between the induction field scan for the old and new GEM1. Here, the effect of a shift in the onset of secondary discharges is rather negligible as it can be seen in Fig. 17, since considering the uncertainties the two measurements are consistent with each other.

On the contrary, a shift of the onset of secondaries for the transfer field for different foils as GEM1 can be observed in Fig. 17, the empty red and green symbols represent

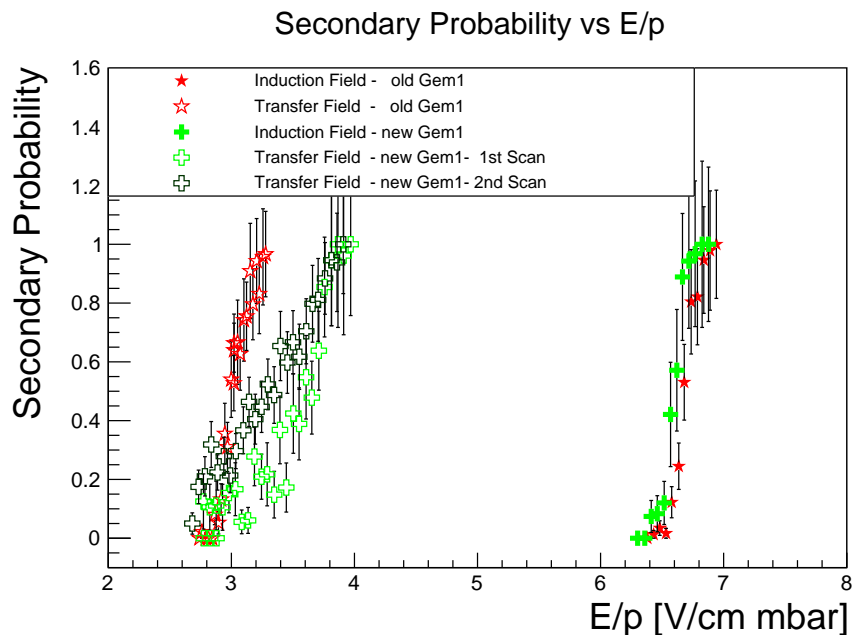


Figure 17: The secondary probability for different foils in the location of GEM1, the discharges were triggered in GEM2.

this comparison. Although, as mentioned above, it is still GEM2 which discharges. However, there is some difference already between two scans conducted with exactly the same settings, represented in light green crosses and dark green crosses. Additionally, during the exchange of the GEM a slight change in the width of the transfer gap might have happened, which would cause a different electric field for the same voltage settings. Considering the uncertainties just described it is not possible to conclude whether the exchange of GEM1 influences the secondary probability significantly or not.

Here, the difference of the electric field necessary for a 50 % discharge probability is

Scan	GEM1	U_{GEM1} [V]	U_{GEM2} [V]	Electric Field $\left[\frac{\text{V}}{\text{cm}\cdot\text{mbar}}\right]$
Induction Field	old	260 V	420 V	0.5
Transfer Field	old	260 V	420 V	1.1
Induction Field	new	257 V	430 V	0.5
Transfer Field	new	259 V	417 V	1.2
Transfer Field	new	262 V	419 V	1.2

Table 2: Overview of settings for Fig. 17. The electric field in the last column describes either the induction field or the transfer field, always complementary to the scanned field. The detailed settings can be found in Appendix A in Tab. 6, Tab. 7, Tab. 15, Tab. 16 and Tab. 17.

around $0.2 \frac{\text{V}}{\text{cm}\cdot\text{mbar}}$.

Comparing the exchange of the two foils one can say that the foils themselves influence the secondary discharge probability in the electric fields created by them, i.e. the electric field below and above the foil. Whether this is independent from if the GEM triggers the discharges or not has to be further investigated. However, discharges in fields that are below or above another GEM of the stack, which was not exchanged, do not seem to be influenced. This was expected, since properties of GEM1 should not affect processes in the induction gap.

This result also means that if a certain configuration of voltages is determined, which allows to operate the GEM stack of the TPC without discharges, the influence of the single foils always has to be taken into account and therefore a certain safe margin has to be kept. The studies conducted within this work are however not yet extensive enough to predict a precise number of how large the safe margin should be.

3.3.2. Different Decoupling Resistors

Another parameter that was studied was the so called 'decoupling' resistor, a resistor that was soldered to the HV supply path of the bottom sides of both GEMs as shown in Fig. 18. The name represents the fact, that these resistors decouple the HV supply and the GEM, i.e. sudden changes in voltage of either of them will only result in a slow rise of voltage in the other component due to the charging curve of a resistor and a capacitor in one circuit. Corrections of the voltage reaching the GEM for the application of the HV probes, just as described before for the top sides see Eq. 4, were not necessary, since the deviation through the decoupling resistor was too small to have an impact.

The values of the decoupling resistors were 11 k Ω , 51 k Ω and 100 k Ω . Both the transfer field and the induction field were scanned with each of the resistors. The settings for both of these measurements can be found in Tab. 3.3.2, during all of the measurements it was GEM2 triggering the discharges.

Transfer Field

The results obtained for the transfer field scan are depicted in Fig. 19. The secondary probability is shown as a function of the transfer field divided by the pressure. There are four measurements represented in the graph, one without a decoupling resistor and three with decoupling resistors of 11 k Ω , 51 k Ω and 100 k Ω respectively. Comparing the measurement without any resistor, which is represented by black, to the other measure-

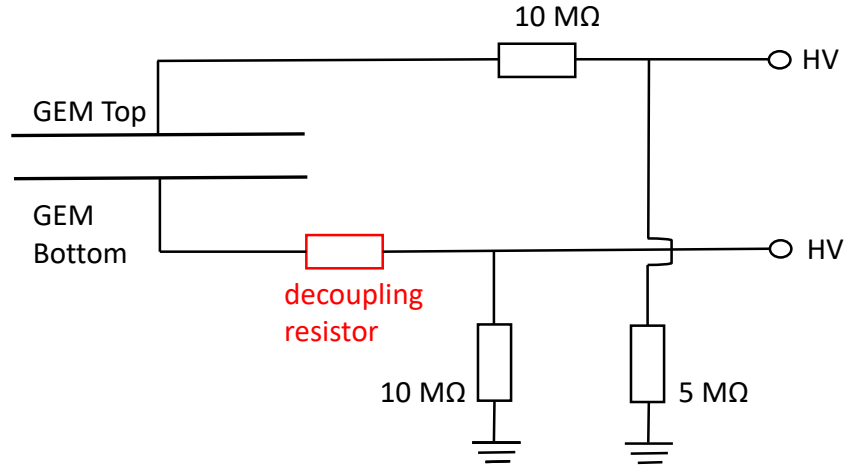


Figure 18: Position of decoupling resistor at the GEM bottom HV supply path.

ments, it becomes clear, that the onset of secondaries of these measurements are clearly shifted towards higher fields. Moreover, examining the other measurements reveals, that this shift is larger, the higher the value of the decoupling resistor is. The secondary onset for a setup with a decoupling resistor of 100 k Ω , represented by blue, is at a transfer field of around $E_T = 4.7 \frac{\text{V}}{\text{cm}\cdot\text{mbar}}$ which differs from the transfer field for the onset without a decoupling resistor by roughly $2 \frac{\text{V}}{\text{cm}\cdot\text{mbar}}$. However, the uncertainties described in chapter 3.3.1 have to be considered, although the uncertainties here are smaller, since no GEMs were exchanged in between and thus the gap widths were not altered.

Induction Field

Likewise the induction field was scanned for different decoupling resistors. The results obtained are presented in Fig. 20. Here, the same colour coding as before applies, i.e. black represents no additional resistor, red an additional resistor of 11k Ω , green 51 k Ω and blue 100 k Ω . Alike the graph discussed before, this graph reveals that there is a clear dependence of the onset of secondaries from the decoupling resistors, since it is shifted towards higher fields for larger values of the decoupling resistors. The difference between the setup with no resistor and the setup with a resistor value of 100 k Ω is around $1.5 \frac{\text{V}}{\text{cm}\cdot\text{mbar}}$, due to the uncertainties described above. It is about the same for scans.

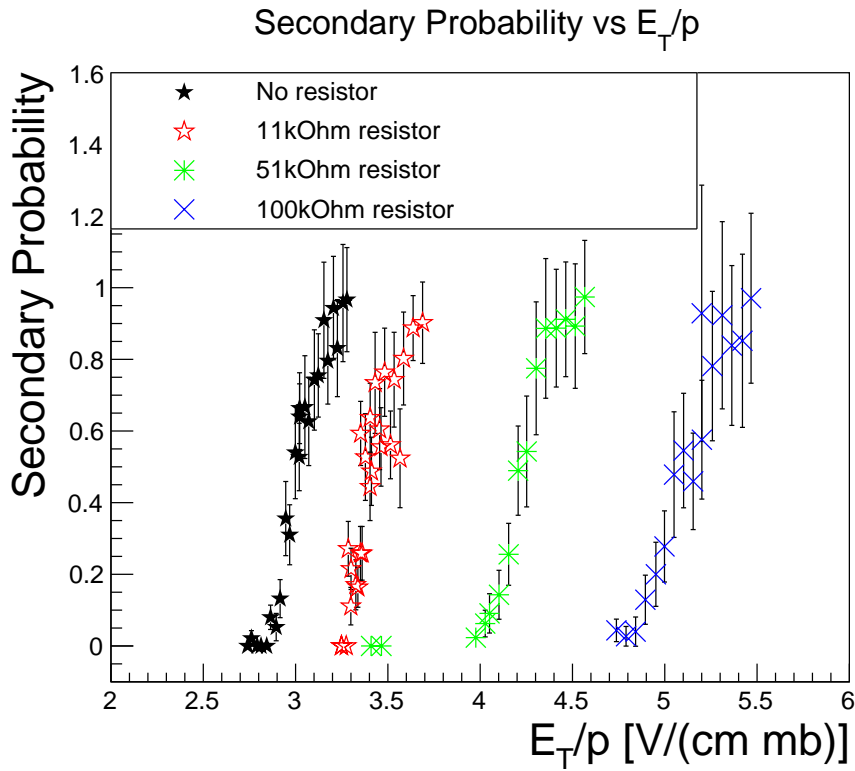


Figure 19: Transfer field scan for different decoupling resistors.

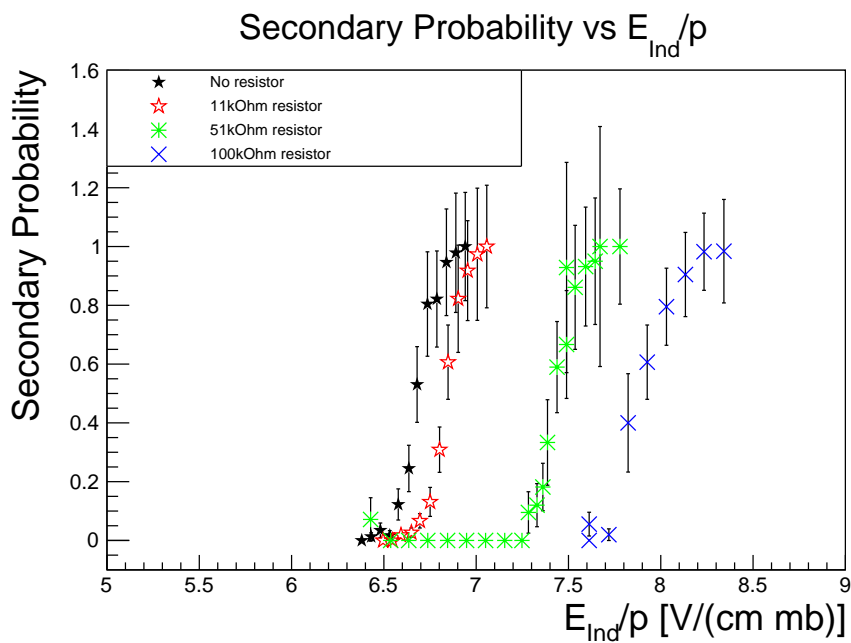


Figure 20: Induction field scan for different decoupling resistors.

Scan	decoupling resistor [k Ω]	U_{GEM1} [V]	U_{GEM2} [V]	Electric Field [$\frac{V}{cm\cdot mbar}$]
E_T	none	260	420	1.2
E_T	11	257	419	1.2
E_T	51	259	421	1.1
E_T	100	260	419	1.2
E_{Ind}	none	257	435	0.5
E_{Ind}	11	246	440	0.4
E_{Ind}	51	263	425	0.7
E_{Ind}	100	257	425	0.8

Table 3: Settings for the results presented in Fig. 19 and Fig. 20. The detailed settings for the transfer field scans be found in Appendix A Tab. 6, Tab. 8, Tab. 11 and Tab. 13 , the detailed settings for the induction field scans in Tab. 7, Tab. 10, Tab. 12 and Tab. 14.

These two measurements demonstrate that decoupling resistors soldered to the bottom sides of the GEMs allow for the application of a certain higher electric field between them, or between the GEM and the readout plane, without having secondaries. Or if the same voltage is applied as before, the secondary probability decreases and therefore allows a more stable and safe operation of the GEMs.

Comparison with Measurements conducted with other Detectors

Furthermore, a comparison of the two scans reveals that the onset of secondaries in the induction field is shifted towards higher fields compared to the onset of secondaries in the transfer field. This might be related to the fact, that during a primary discharge and the subsequent potential drop of GEM2 top the transfer field is increased by $\mathcal{O}(2 \frac{V}{cm\cdot mbar})$, so the actual transfer field is higher than the one that is adjusted. This, however, needs to be further investigated. Since, as described before, the gas mixture of the future TPC will be different from the gas used for these experiments, the direct comparison of the onset electric field of the secondaries with the electric fields planned for the four GEM stack of the TPC is not possible. Nevertheless, it is possible to derive some conclusion, also from earlier measurements that were conducted with both gas mixtures, which can be used as reference. This will be discussed in more detail in 3.4.

From Fig. 20 and Fig. 19 the information of the electric field necessary for a 50% secondary discharge probability in dependence of the resistor can be obtained. This dependency is depicted in Fig. 21. It indicates that there is a linear correlation between the electric field for a certain secondary probability and the resistor value. Blue represents the fit for the induction field and red the fit for the transfer field scan. The

slope is $(0.020 \pm 0.001) \frac{\text{V}}{\text{cm}\cdot\text{mbar}\cdot\text{k}\Omega}$ for the transfer field and $(0.012 \pm 0.001) \frac{\text{V}}{\text{cm}\cdot\text{mbar}\cdot\text{k}\Omega}$ for the induction field. The larger slope of the transfer field scan in contrast to the slope of the induction field scan could also indicate that the decoupling resistors have a larger impact on the secondary probability in the transfer field than in the induction field.

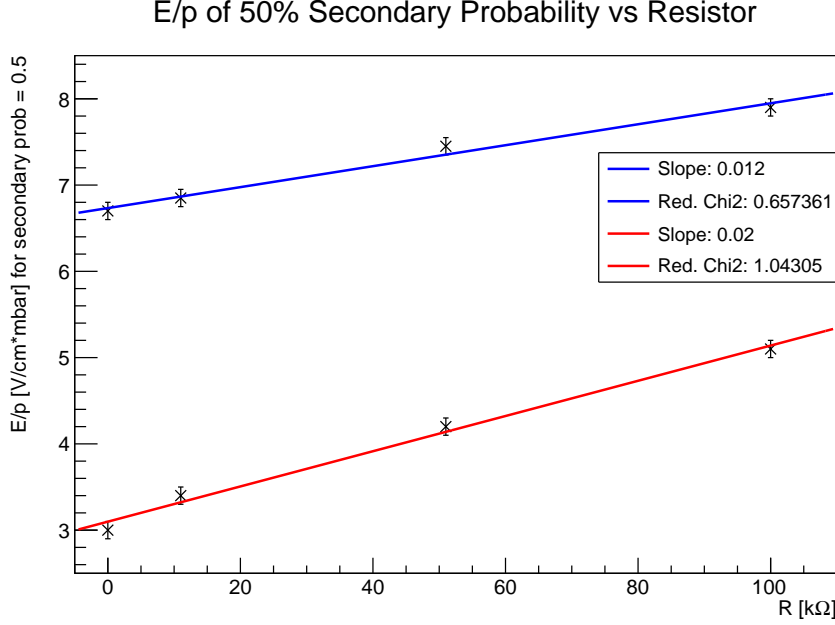


Figure 21: Electric field (over pressure) for which the secondary probability is 50% as a function of the resistor value. The blue line is the fit for the induction field and the red line for the transfer field.

The result that the electric field for a certain secondary probability depends linearly on the value of the resistor is in agreement with earlier measurements executed by P. Gasik in Munich with a one GEM detector [26]. In Fig. 22 these results are presented, the onset field is shown as a function of the value of the decoupling resistor. Here, the different symbols indicate different loading resistors, which, in the measurements presented here, is constant 10 MΩ. The slope of the measurements in Munich is around $0.015 \frac{\text{V}}{\text{cm}\cdot\text{mbar}\cdot\text{k}\Omega}$, so the order of magnitude for the two measurements is the same, which means they agree well. Consequently, the linear correlation between the field for a specific secondary probability and the decoupling resistor value might also be valid for all fields in a stack of four GEMs.

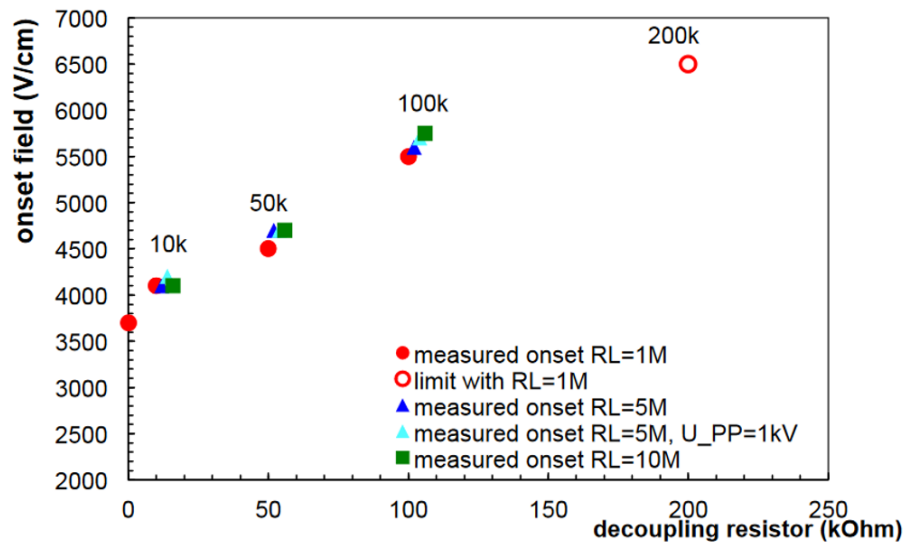


Figure 22: Measurements with a one GEM detector executed in Munich. The gas mixture used for these measurements was Ne-CO₂-N₂ 90-10-5 [26].

Observation of Properties of Primary and Secondary Discharges

During the measurements described above, different properties of the primary and secondary discharges were examined. These include

- amplitude height at the readoutplane
- time difference
- potential changes of the GEMs during discharges
- propagation probability

Below, these terms and the observations are described in more detail.

Amplitude

One of these properties is the amplitude height of the signal of primary and secondary discharges measured at the readout plane. Measurements conducted without decoupling resistors showed that the attenuated amplitude of the primary discharge is considerably smaller than the attenuated amplitude of the secondary discharge, see Fig. 23.

However, with the decoupling resistor soldered to the HV supply path, the amplitudes approached each other: The secondary amplitude decreased, while the primary amplitude stayed the same or even increased a little. This led to the problems of the counter logic as described above.

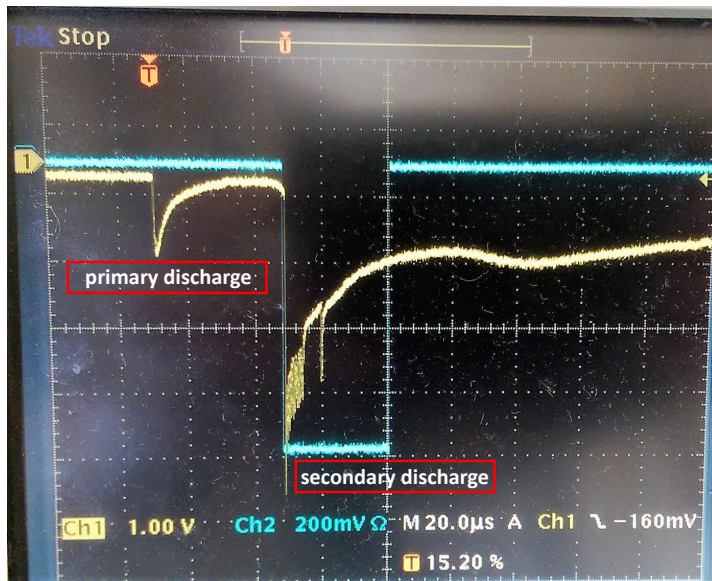


Figure 23: Picture of oscilloscope screen. The yellow signal is the signal from the readout plane. Blue is the signal from the secondary gate, which was described in 14. The difference of the amplitudes of primary and secondary discharge is clearly visible.

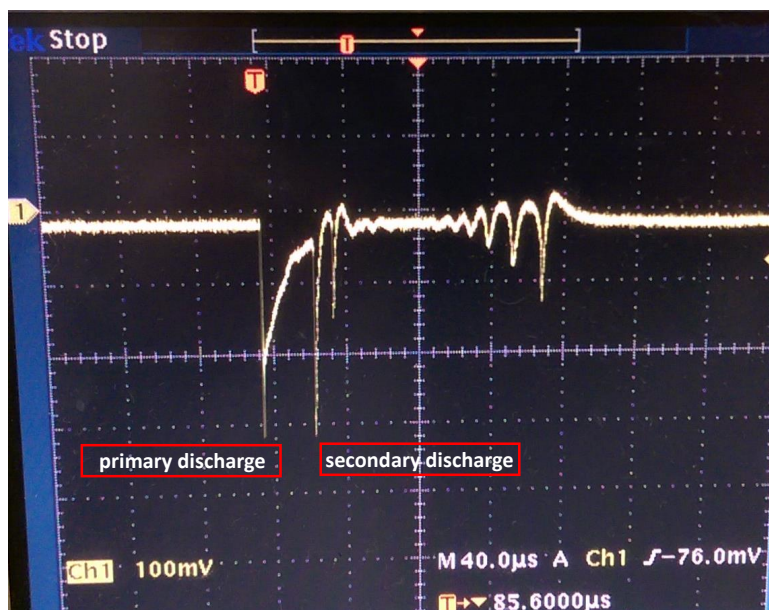


Figure 24: Picture of oscilloscope screen. The yellow signal is the signal from the readout plane. This was measured with a $51\text{ k}\Omega$ decoupling resistor. Here the amplitudes of the primary and secondary signal have the same height.

For three settings, two of them with no decoupling resistors and one with 11 k Ω decoupling resistors, it was possible to calculate the mean primary and secondary amplitudes, which are presented in Tab. 4. The mean was obtained from data recorded by the oscilloscope and with the help of C++ analysis scripts the amplitude heights were extracted.

measurement	primary amplitude	secondary amplitude	resistor
1	(-0.33 ± 0.01)	(-0.40 ± 0.08)	none
2	(-0.33 ± 0.01)	(-0.57 ± 0.06)	none
3	(-0.47 ± 0.01)	(-0.42 ± 0.05)	11 k Ω

Table 4: Mean amplitude height

It can be derived from these values, that the amplitude of the primary discharge even slightly increases with a decoupling resistor. However, it is not possible to extract from these data a clear dependence of the secondary discharge amplitude on the decoupling resistor. Nevertheless, observations reveal that the secondary discharges decrease significantly, so this should be further examined.

Time Difference

Moreover, it was examined, how the time between secondary and primary discharges depends on the electric field. It was observed that the higher the field, the shorter the time between primary and secondary discharges became, as it can be seen in Fig. 25 and Fig. 26. A similar dependence was observed in previous measurements, examining secondary discharges in the induction gap. This might be a hint concerning the origin of secondary discharges, it seems like whatever causes them is charged, since it becomes faster for a higher field. The drift velocity of ions is $v = E \cdot (1.8 \pm 0.2) \frac{\text{cm}}{\mu\text{s}}$ [27] and hence around $0.005 \frac{\text{cm}}{\mu\text{s}}$ for an electric field of $E = 2.9 \frac{\text{kV}}{\mu\text{s}}$. So the time for ions to travel the distance of the transfer or induction gap, which is 2 mm wide, is around 40 μs . This is very close to the measured time difference between a primary and secondary discharge for this electric field, which is roughly around 25 μs .

However, also observations have been made, that point directly to the opposite conclusion, namely that the behaviour of the discharges in the transfer gap is the same for a reversed field [28]. This indicates, that the reason for discharges is not charged, since it is not influenced by the direction of the electric field. These two contradictory observations reveal that there is still little knowledge about the causes for secondary discharges, so further investigations on this topic are necessary.

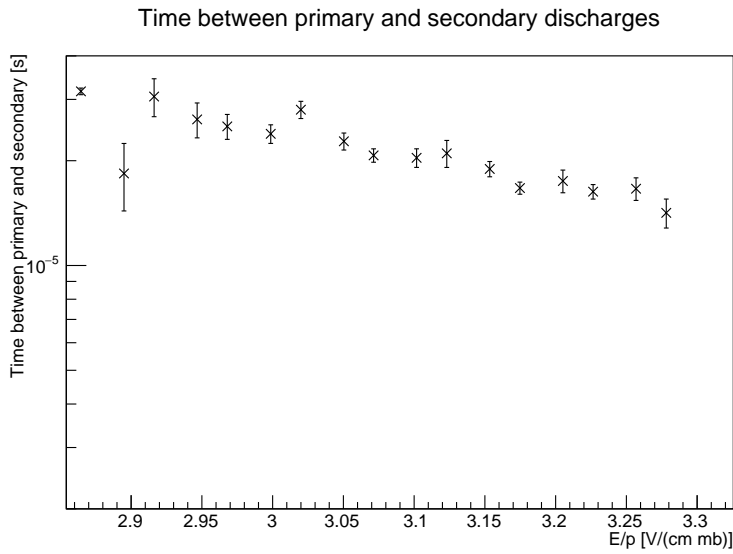


Figure 25: Time difference between primary and secondary discharges in dependence of the electric field over the pressure. Setup with no decoupling resistor. Transfer field scan with discharges triggered in GEM2.

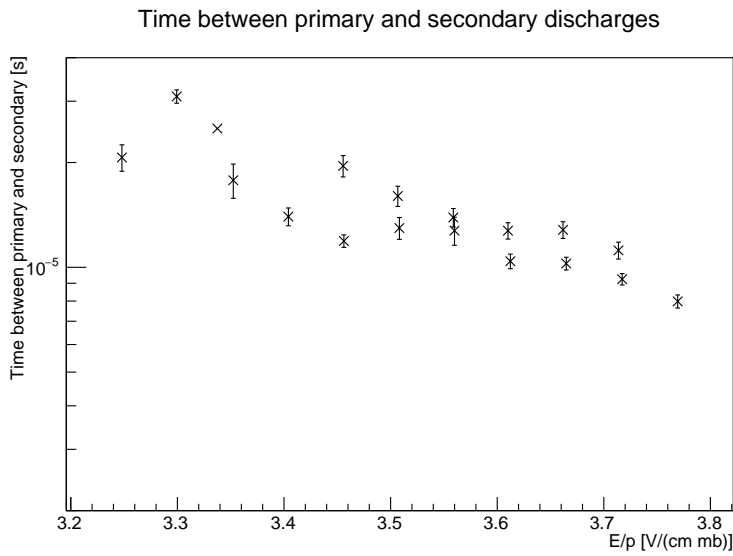


Figure 26: Time difference between primary and secondary discharges in dependence of the electric field over the pressure. Setup with 11 k Ω . Transfer field scan with discharges triggered in GEM2.

The uncertainties of the measurements were calculated according to Gaussian or Poisson uncertainty. The deviations between points in Fig. 26 indicate, that the uncertainties of the measurements are larger than expected, this has to be considered as well.

Potentials

Another important aspect of discharges is how they change the potentials on the GEM electrodes. In the standard configuration, i.e. with no decoupling resistor and a 10 M Ω resistor at the top side, a discharge will cause the drop of the top side potential on the bottom side potential. As explained before, this, together with the segmentation of the top side of the GEMs, ensures that only a small part of the whole GEM will be affected by the discharge. However, with decoupling resistors and secondary discharges the behaviour of the potentials becomes more complex. The potentials are examined, as described before in chapter 3.1 with HV probes, the signal on the oscilloscope is proportional to the actual voltage of the GEM.

GEM1 potentials

In Fig. 27 the potentials of GEM1 during a discharge in GEM2 are depicted. GEM1 top is represented by blue and GEM1 bottom by yellow. In this example we see that the top potential drops closely towards the bottom potential, as it is the case for the setup without decoupling resistor. Nevertheless, the bottom potential drops as well, roughly about the same amount as the top potential, which was not the case for the measurements conducted without decoupling resistor. During the secondary discharge both potentials drop further, most likely on the same potential, since these pictures could not be corrected for the different AC responses of the HV probes. Afterwards, both potentials recover together, i.e. approach their original potentials.

GEM2 Potentials

In Fig. 28 the potentials of GEM2 during a discharge in this GEM are depicted. Since the oscilloscope had only two channels, Fig. 28 and Fig. 27 do not present potentials of the selfsame discharge. However, both show discharges of the same setup and with the same settings. Also the colours are interchanged, GEM2 top is yellow and GEM2 bottom blue. For the primary discharge there is a clear drop of the GEM2 top potential, the GEM2 bottom increases in contrary to the GEM1 bottom potential. With the secondary discharge both potentials together increase, towards GEM1. Then, after some oscillations, both potentials drop again. Finally they start to recover. An interesting

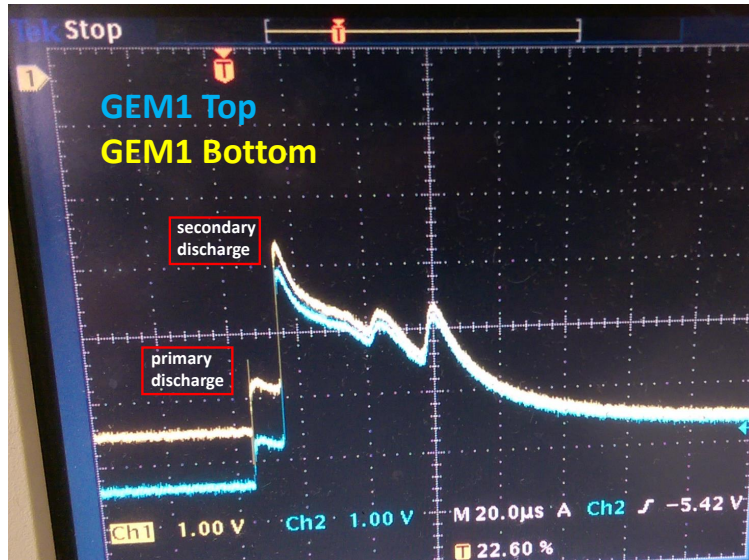


Figure 27: GEM1 potentials during a primary and secondary discharge. Blue represents GEM1 top and yellow GEM1 bottom. The discharge is triggered in GEM2. This setup included a decoupling resistor of 100 k Ω .

observation is, that during the primary discharge the GEM potentials meet just in the middle between the top and bottom potential, instead of the top potential simply dropping on the bottom potential, as described before it is the case without resistors. If a primary discharge like this happened in a four GEM stack, not just one part of the segmented top side, but all of the GEM would be affected, since the potential of the unsegmented bottom side is also changed. This would then affect as well the electric field below the GEM. However, it has also to be kept in mind, that a secondary discharge, which has as described above a higher probability to occur without a decoupling resistor, would nevertheless change the bottom potential.

Potentials during Discharge in Transfer Gap

Additionally, it is interesting to observe the GEM1 bottom and GEM2 top potential during a discharge in the transfer gap. This can be seen in Fig. 29. Both potentials drop after the primary discharge. During the secondary discharge the GEM1 bottom potential drops further, however the GEM2 top potential increases, so both potentials approach each other. Moreover, some time after the secondary discharge oscillations in both channels occur. This phenomenon appeared regularly during the measurements and can be seen as well in Fig. 28. Observations and the comparison of a lot of recorded oscilloscope screens indicate that these oscillations have a longer duration with a higher value of the decoupling resistor. Additionally, it seems like the frequency is also

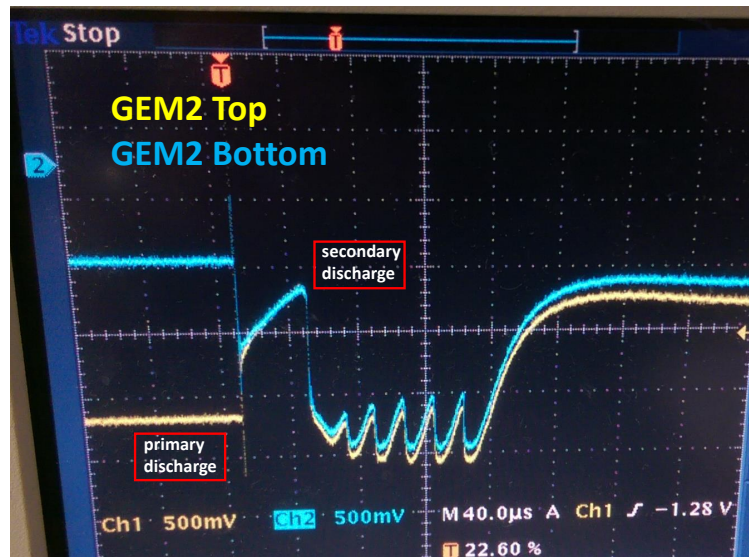


Figure 28: GEM2 potentials during a primary and secondary discharge. Yellow represents the GEM2 top and blue GEM2 bottom. The discharge is triggered in GEM2. The setup included a decoupling resistor of 100 k Ω .

influenced by the value of the decoupling resistor, however, these measurements were not extensive enough with respect to this phenomenon to conclude detailed dependencies.

Potentials during Discharge in Induction Gap

To complete the observations on the potentials in Fig. 30, the potentials during a discharge influencing the induction gap are depicted. The setup for this discharge also included a 51 k Ω decoupling resistor. After the primary discharge, a drop of the GEM2 bottom potential, as well as a drop in the GEM1 top potential is seen. In contrary to the secondary discharge in the transfer field, the secondary discharge in the induction field leads to a further drop of the GEM2 potential. Moreover, the GEM1 top potential is only slightly affected and recovers very fast to its original potential.

To sum up the observations of the potentials, one can say, that usually during a primary discharge all the potentials drop, except for the GEM2 bottom potential during a discharge in the transfer field. The potentials for the secondary discharge behave differently, depending on whether the secondary discharge happens in the transfer or in the induction field. For a secondary discharge in the transfer field, the potentials of GEM1 and GEM2 approach each other, whereas for a secondary discharge in the induction field the potentials drop further. Additionally, it was observed that the longest recovery times of the potentials, i.e. the time until they reach their initial values again, are in the order of ms.

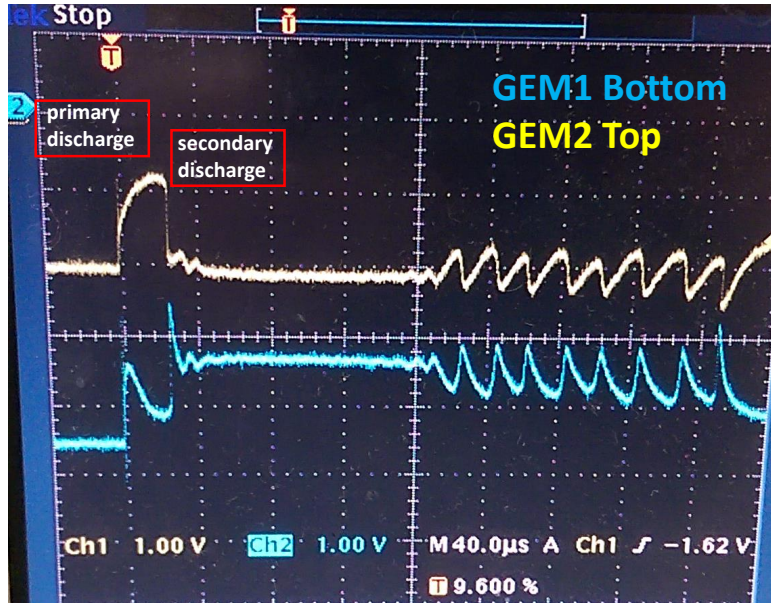


Figure 29: GEM potentials during a primary and secondary discharge. Blue represents the GEM1 bottom and yellow GEM2 top. The discharge is triggered in GEM2. **Transfer field** scan with decoupling resistor of 51 k Ω .

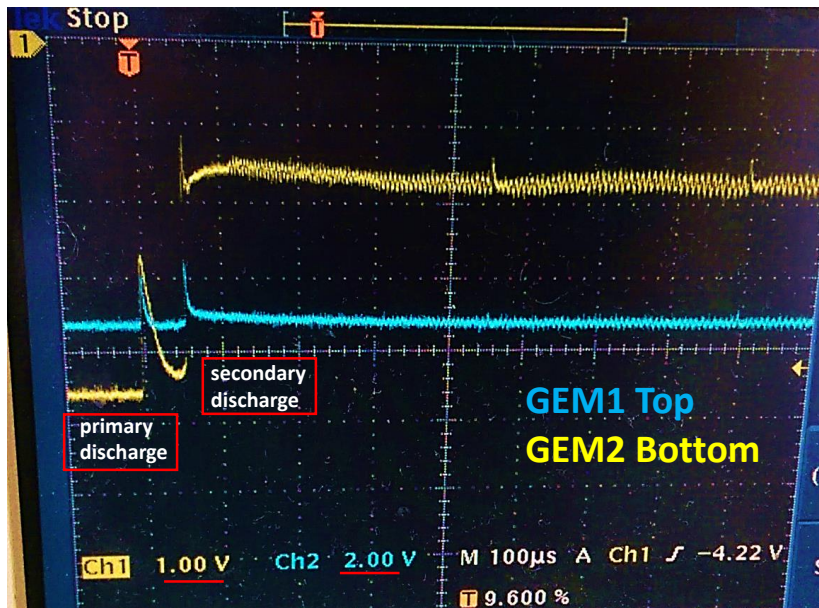


Figure 30: GEM potentials during a primary and secondary discharge. Blue represents the GEM1 top potential and yellow the GEM2 bottom potential. The discharge is triggered in GEM2. **Induction field** scan with decoupling resistor of 51 k Ω . The two channels have different voltage scales.

Propagation Probability

Observing discharges in a stack led to the conclusion that discharges triggered in one GEM sometimes cause discharges in other GEMs as well, i.e. the discharge propagates from one GEM to the other GEM. Hence, during the analysis also the propagation probability was extracted from the data. Therefore, the GEM potentials before and after the primary discharge were compared. In order to do so a fit of the potentials was executed and the obtained values were subtracted. These results were written into histograms. From the histograms the propagation probability for GEM1 top and the probability of a potential change for GEM1 bottom and GEM2 was then simply calculated by

$$P_{change} = 1 - \frac{N_0}{N_{tot}}, \quad (6)$$

with N_0 representing the entries without any potential change and N_{tot} the total number of entries. Due to a limitation of data samples this could only be examined for GEM2 discharging and for transfer field scans.

In Fig. 31 and Fig. 32 the probability of a change of the potential after the primary discharge in GEM2 as a function of the electric field is depicted for GEM2 and GEM1. Since GEM2 is discharging we see the expected behaviour of the GEM2 potentials: The primary discharge causes the top potential to drop on the bottom potential, hence the probability to change is for all electric fields around 100 % for the top potential and around 0% for the bottom potential. However, examining the GEM1 potentials reveals new information: From the graph it becomes clear, that there is a propagation probability of around 100 % no matter what electric field is applied. This means, that whenever a discharge is triggered in GEM2 this causes a discharge in GEM1 as well. For higher fields even the GEM1 bottom potential seems to be affected.

In Fig. 33 and Fig. 34 the same dependencies as described above are depicted, just for a setup with an additional 11 k Ω decoupling resistor. For GEM2 top the probability of a potential drop is still 100 %, which is reasonable since the discharges are triggered in this GEM. For GEM2 bottom, however, we see a difference compared to the discharges without a decoupling resistor. For increasing fields the probability that the GEM2 bottom potential is altered increases. This is in agreement with the observations of the potentials of the GEMs described in the paragraph above.

The propagation probability extracted from Fig. 34 for discharges propagating from GEM2 to GEM1 is again around 100 % for higher fields, with a slightly lower probability for lower fields, which is only around 60 % to 80 %. With this setup the GEM1 bottom potential is even more affected by a discharge in GEM2 than before, the probability

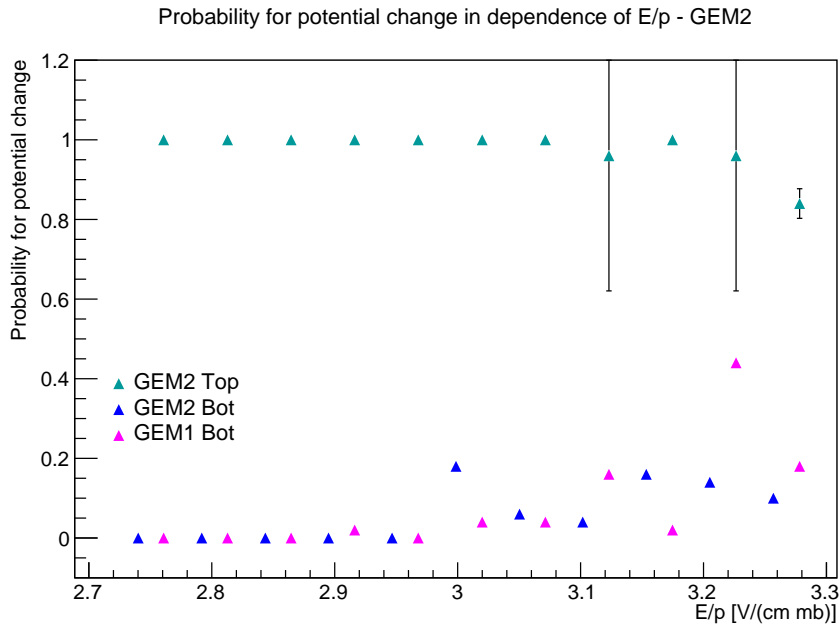


Figure 31: Probability that the potentials are altered after a primary discharge in GEM2 in a setup with no decoupling resistor. Light and dark blue represent GEM2, magenta represents GEM1 bottom.

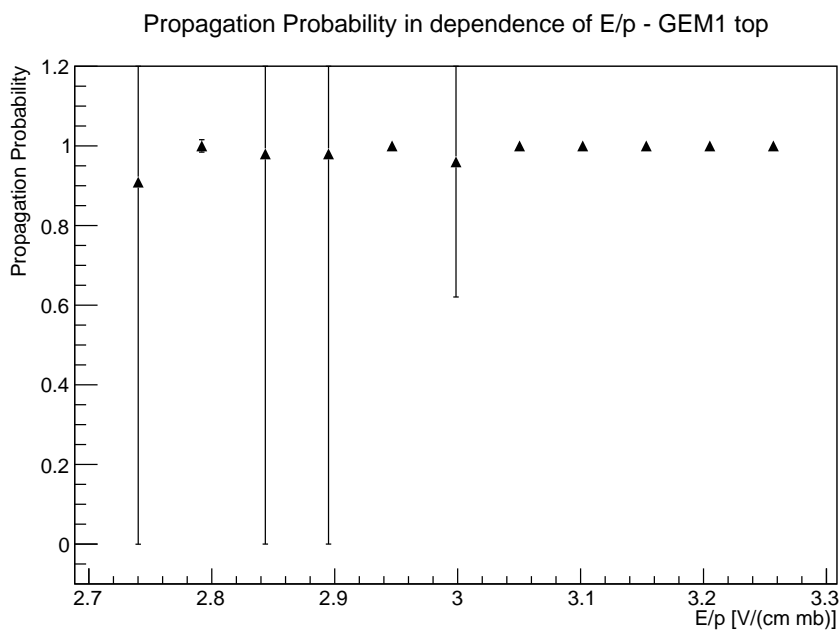


Figure 32: Propagation probability in a setup with no decoupling resistor and discharges triggered in GEM2..

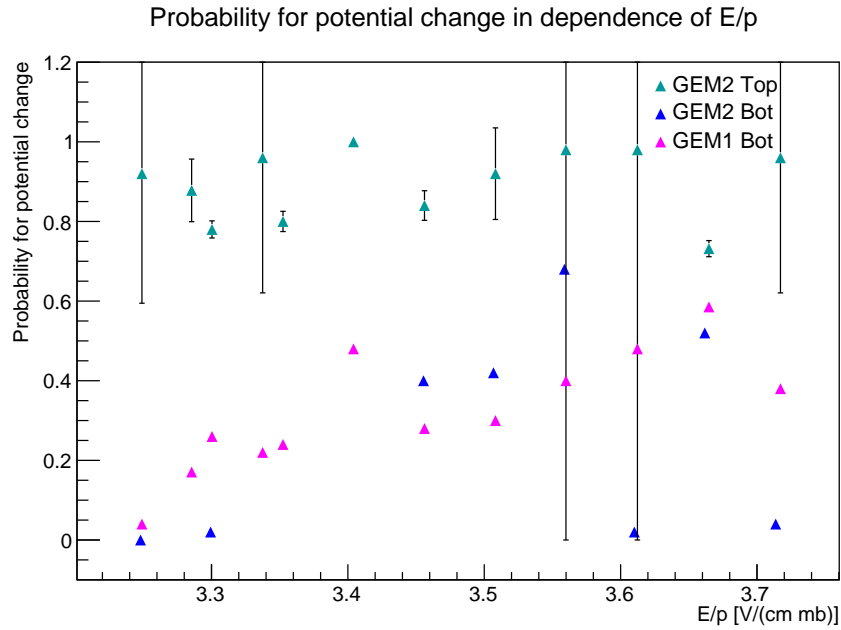


Figure 33: Probability that the potentials are altered after a primary discharge in GEM2 in a setup with 11 k Ω decoupling resistor. Light and dark blue represent GEM2, magenta represents GEM1 bottom.

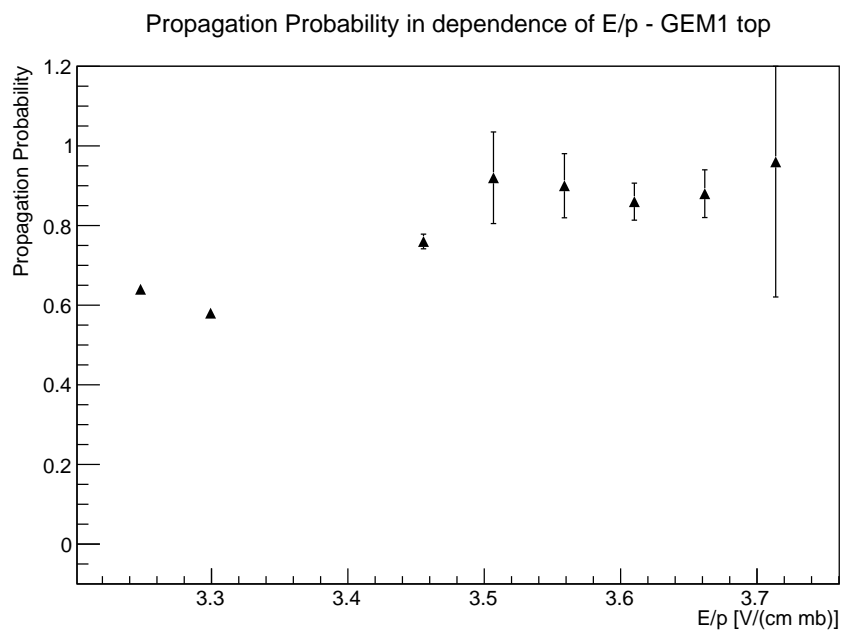


Figure 34: Propagation probability in a setup with 11 k Ω decoupling resistor and discharges triggered in GEM2.

increases for higher fields from around 20% to 60%. This resembles the behaviour of the GEM2 bottom potential and probably as well due to the decoupling resistor.

All in all, the propagation probability for the examined measurements is really high, reaching around 100 % nearly independent of strength of the electric field between GEM1 and GEM2. So discharges in GEM2 have a great impact on GEM1. However, other parameters that might affect the propagation probability, have not been studied.

3.3.3. Discharges triggered by GEM1

The last parameter that was investigated was the influence of triggering the discharges in GEM1 instead of GEM2. This was achieved by basically interchanging the voltages across the two GEMs, i.e. applying a voltage of more than 400 V at GEM1 and around 250 V at GEM2. In Fig. 35 measurements for GEM1 triggering discharges and GEM2 triggering discharges are compared for a transfer field scan. A transfer field scan was conducted for both measurements. This graph shows again the secondary probability in dependence of the electric field over the pressure. Analysing the two scans it becomes clear, that the secondary onset is shifted towards higher fields for GEM1 discharging compared to discharges triggered in GEM2. The divergence of the onset is about $0.7 \frac{\text{V}}{\text{cm}\cdot\text{mbar}}$.

As described before, during a primary discharge without a decoupling resistor only the top potential is influenced. This means that there is the possibility that if GEM1 discharges, the field between the two GEMs is not affected. Yet, it is possible that the discharge of GEM2 influences the field between the two GEMs, increasing it to a higher value than the set one, by adding the voltage difference across GEM2 to the transfer field. For $\Delta U_{GEM2} = 400 \text{ V}$ this adds $E_{add} = 2 \frac{\text{V}}{\text{cm}\cdot\text{mbar}}$ to the transfer field. Since the difference of onset is smaller than this, there are probably more factors that influence the shift of the onset. This is of course only true for a two GEM stack, as soon as the upper GEM has another GEM above, the field between them is distorted by a potential drop of the upper GEM top side as well. So the least distortion in a four GEM stack would be caused by the uppermost GEM discharging. However, the voltage across this GEM has to be rather low to keep the ion back flow small. Additionally, discharges in this GEM could propagate to the other GEMs of the stack.

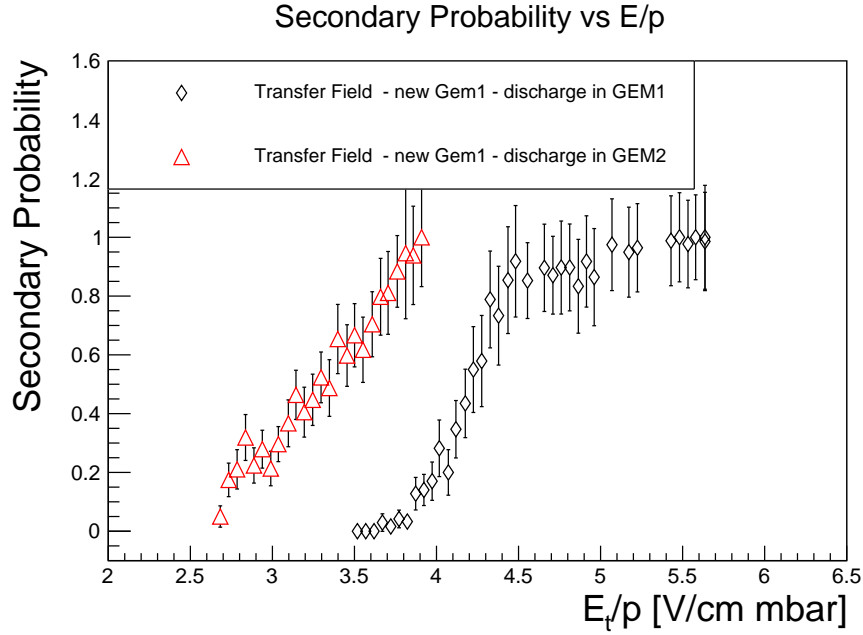


Figure 35: Discharges triggered in GEM1 compared to discharges triggered in GEM2 for a transfer field scan. The detailed settings can be found in Appendix A Tab. 15, Tab. 16, Tab. 18 and Tab. 19

Potentials

The potentials of GEM2 during discharges in GEM1 reveal an interesting correlation. This is illustrated in Fig. 36, the GEM2 top potential is yellow and the GEM2 bottom potential is blue. It can be seen, that during the primary discharge of GEM1 no discharge occurs in GEM2. However, there is a secondary discharge which then also influences the GEM2 potentials. Fig. 37 shows the GEM2 potentials as well, however, this time the primary discharge in GEM1 triggers a discharge in GEM2. Although the preconditions are altered compared to the above described discharge there again is a secondary discharge. This suggests, that no matter if GEM1 induces a discharge in GEM2 or not, there is the possibility of a secondary discharge. Further investigations can be considered concerning a dependence of the secondary probability on whether the primary discharge in GEM1 induces a discharge or not in GEM2.

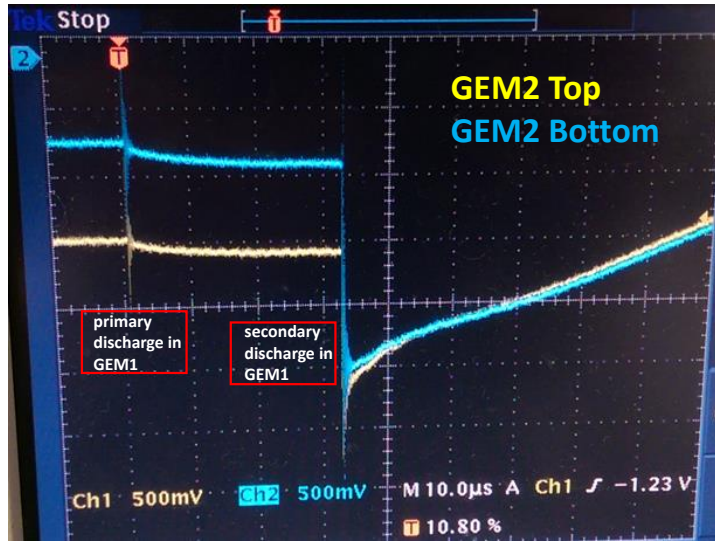


Figure 36: Potentials of GEM2 during discharges triggered in GEM1. Setup with no decoupling resistor. Transfer field scan.

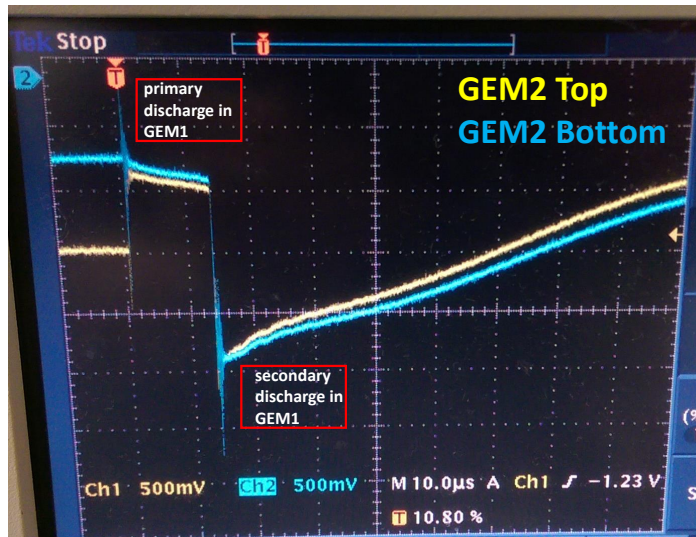


Figure 37: Potentials of GEM2 during discharges triggered in GEM1. Setup with no decoupling resistor. Transfer field scan.

3.4. Discussion

Three parameters were examined for their influence on secondary discharges, the influence of a foil itself, additional decoupling resistors and the location of the discharging GEM. The presented results are, as described before, obtained for measurements in a gas composed of argon and carbon dioxide. However, the gas inside the upgraded TPC will be a mixture of neon, carbon dioxide and nitrogen. Other measurements revealed that the discharge probability is different for different gases [29]. Due to the fact that the cause for discharges, especially secondary discharges, is not yet completely known, there is no possibility of a simple conversion from the results obtained with one gas mixture to another gas mixture. Hence, to obtain detailed values of secondary onsets the same measurements should be executed in the gas mixture of the future TPC. Nevertheless, these results allow for a quantitative comparison with the neon gas mixture, considering results from measurements conducted with different gas mixtures. The conversion factor to obtain the same gain in Ar-CO₂-N₂ as in Ne-CO₂-N₂ is about 1.2 [30]. However, studies on discharges conducted with the two different gas mixtures revealed, that the onset differs not simply by a factor of 1.2.

The configuration of the four GEM stack implies, as described in chapter 2.2.2, two strong fields with $E_T = 4.0 \frac{\text{kV}}{\text{cm}}$. These are the critical fields, where a certain secondary probability is possible, since for Ar-CO₂ the onset was around $E_T = 2.9 \frac{\text{kV}}{\text{cm}}$. In the case of further investigations confirming that the secondary onset is already reached with these fields in Ne-CO₂-N₂, additional decoupling resistors should be considered in order to operate the GEM stack safely. As mentioned before this affects the potentials after a primary discharge, however, the advantage of the decoupling resistor, to reduce the probability of secondary discharges, is clearly predominating.

4. Summary and Outlook

Within this thesis the influences of different parameters on the secondary discharge probability were examined. It is important to understand the impact and origin of the discharges in order to ensure a safe operation of GEMs in the readout chambers of the upgraded ALICE TPC. The results of investigating the different parameters are shortly summarized in the following.

Influence of GEM Foil itself

When comparing the same setup just with different foils it became clear, that the foil itself has an impact on the secondary discharge probability, since the onset of secondaries is shifted towards different values of the electric field for different foils. Hence, a safe margin has to be kept when determining a configuration without secondary discharges for the foils. The studies presented here are however not extensive enough to provide a precise number for this safe margin.

Decoupling Resistor

An additional resistor in the HV power supply path for the GEM bottom sides had several impacts on the secondary discharge probability. There was a clear dependency of the secondary onset on the value of the resistor, the higher the value the more the onsets of the secondaries were shifted towards higher fields. This proved to be a linear correlation. Additionally the resistors have an impact on the behaviour of the GEM potentials which drop and increase slightly differently compared to a setup with no additional resistor. Moreover, plotting the time between primary and secondary discharge against the electric field reveals that this time difference becomes smaller with growing electrical field, indicating that what causes secondaries might be charged. However other observations are contradictory to the simple picture of e.g. moving ions. It was also observed that the propagation probability, the probability that a discharge in one GEM triggers a discharge in the other GEM, is about 100 % for a setup with no decoupling resistor, as well as for a setup with a decoupling resistor.

So the additional resistor allows for a safer operation of a single GEM, since it decreases the secondary probability significantly. However, for an operation within a stack, the fact that this resistor alters the GEM bottom potential is an unwanted effect, since this influences the field under the foil, in contrast to the current configuration where only the field above is influenced by a primary discharge. Since as already discussed, some of the fields planned for the configuration of the stack inside the TPC are higher than the

field needed in Ar-CO₂ for a secondary onset, it should be considered if less secondaries but a changing GEM bottom potential is not the better option.

Location of GEM starting the Discharges

Inducing discharges with either GEM1, in our case the upper GEM, or GEM2 revealed that the location of the GEM used to trigger the discharges influences the propagation probability. This is concluded from the fact that the onset of secondaries for GEM1 triggering discharges is shifted towards higher electric fields compared to the onset for GEM2 triggering discharges. Consequently the uppermost GEM discharging in a stack is less problematic than the discharging of other GEMs in the stack. However this GEM has to be operated with a low potential difference in order to keep the IBF low.

Additionally it was observed that primary discharges triggered in GEM1 sometimes cause a discharge in GEM2 (propagate) and sometimes not, however in both cases a secondary discharge can occur. This means, a propagated discharge from GEM1 to GEM2 is no prerequisite for a secondary discharge. Nevertheless, the propagation could influence the secondary probability, which could not be examined in the scope of this work, hence this is something to be further investigated.

Appendix

A. Detailed Settings of Measurements

Here all the measurements described during this work are listed in detail. The time in the first column is the period during which the number of primary (#1) and secondary (#2) discharges are counted. Moreover, the pressure, the temperature and the ratio of gas to water is given in the table. Additionally, the settings of GEM1 and GEM2 and the resulting voltages for the region of the drift field, induction field and transfer field are depicted.

Table 5: Transfer field scan. Old GEM2. No decoupling resistor.

time [s]	#1	#2	p [mbar]	T [°C]	H ₂ O [ppm]	U _{GEM2} [V]	U _{GEM1}	Drift	Ind	T1
200	53	0	979,5	21	129	422	262	1200	198	593
200	58	0	979,5	21	130	422	263	1200	198	603
200	56	0	979,5	21	130	422	261	1200	198	614
200	109	0	979,4	21	129	422	263	1200	198	623
200	65	9	979,4	21	131	422	261	1200	198	634
200	55	11	979,3	21	128	422	262	1200	198	643
200	55	4	979,3	21	130	422	262	1200	198	653
200	56	16	979,2	21	125	422	261	1200	198	664
200	121	86	980,6	22	135	422	256	1200	198	669
200	184	152	980,5	22	136	422	258	1200	198	688
200	145	66	980,4	22	135	422	263	1200	198	650
200	106	10	980,4	22	134	422	261	1200	198	635
200	83	5	980,3	22	136	422	262	1200	198	625
200	125	0	980,3	22	133	422	263	1200	198	614
200	104	0	980,2	22	137	422	262	1200	198	603
200	82	0	980,2	22	135	422	261	1200	198	594
200	104	1	970,9	21	836	421	264	1200	198	604
200	126	6	970,7	21	835	421	265	1200	198	614
200	89	0	970,6	21	836	421	262	1200	198	623
200	75	34	970,8	21	522	421	263	1200	198	664
200	58	52	970,7	21	596	421	263	1200	198	700
200	114	91	970,7	21	636	421	265	1200	198	680

Table 6: Measurements with new GEM2. Transfer field scan. No decoupling resistor.

time [s]	counts #1	counts #2	p [mbar]	T [°C]	H2O [ppm]	U_{GEM2} [V]	U_{GEM1} [V]	Drift [V]	Ind [V]	T [V]
200	47	1	967,1	21	189	420	262	1200	224	534
200	51	0	967	21	183	420	262	1200	224	544
200	75	6	967	21	173	420	262	1200	224	554
200	53	7	967	21	173	420	262	1200	224	564
200	58	18	967	21	175	420	262	1200	224	574
200	91	48	966,9	21	175	420	262	1200	224	584
200	67	42	967	21	175	420	262	1200	224	594
200	98	74	967	21	171	420	262	1200	224	604
200	98	78	967	21	171	420	262	1200	224	614
200	83	69	967	21	170	420	262	1200	224	624
200	90	87	967	21	170	420	260	1200	224	634
200	6	0	967,1	21	165	416	259	1200	222	530
200	10	0	967,1	21	163	416	259	1200	222	540
200	35	0	967,1	21	162	420	258	1200	218	550
200	38	2	967,2	21	160	420	260	1200	218	560
200	45	16	967,2	21	160	420	260	1200	218	570
200	50	27	967,1	21	158	420	259	1200	218	580
200	54	36	967,1	21	157	420	259	1200	218	590
200	66	49	967,2	21	158	420	259	1200	218	600
200	66	60	967,2	21	158	420	259	1200	218	610
200	88	83	967,2	21	156	420	258	1200	218	620
200	70	67	967,2	21	156	420	258	1200	218	630

Table 7: Induction field scan. No decoupling resistor.

time [s]	#1	#2	p [mbar]	T [°C]	H ₂ O [ppm]	U _{GEM2} [V]	U _{GEM1} [V]	Drift [V]	Ind [V]	T [V]
200	58	2	980	20	228	435	259	1200	1270	94
200	60	1	980	20	231	435	258	1200	1280	95
200	49	6	980	20	239	436	256	1200	1289	94
200	49	12	980	20	230	434	255	1200	1300	96
200	49	26	980	20	238	436	256	1200	1309	94
200	46	37	980	20	238	435	256	1200	1320	94
200	56	46	980	20	229	434	255	1200	1330	96
200	56	53	980	20	241	434	255	1200	1340	96
200	47	46	980	20	227	435	255	1200	1350	95
200	59	59	980	20	233	434	256	1200	1360	95
200	63	0	980	20	228	435	259	1200	1250	94
200	77	1	980	20	228	435	258	1200	1260	94

Table 8: Transfer field scan. 11 k Ω decoupling resistor. Part 1.

time [s]	#1	#2	p [mbar]	T [°C]	H2O [ppm]	U_{GEM2} [V]	U_{GEM1} [V]	Drift [V]	Ind [V]	T [V]
200	58	0	968,4	21	167	421	262	1200	223	584
200	49	0	966,8	21	156	421	262	1200	223	584
200	60	0	966,6	21	148	421	262	1200	223	594
200	57	0	966,5	21	143	421	262	1200	223	604
200	96	2	963,8	21	119	421	262	1200	223	614
200	75	6	963,6	21	120	421	262	1200	223	624
200	86	2	963,5	21	119	421	261	1200	223	634
200	92	24	963,4	21	121	421	261	1200	223	644
200	155	95	963,4	21	117	421	261	1200	223	654
200	79	17	960,5	20	820	421	260	1200	223	634
200	118	70	960,5	20	830	421	258	1200	223	644
200	113	72	960,6	20	780	421	259	1200	223	654
200	161	105	960,6	20	800	421	258	1200	223	664
200	139	91	960,6	20	700	421	255	1200	223	674
200	130	82	960,7	20	693	421	253	1200	223	684
200	133	88	960,6	20	697	421	252	1200	223	694
200	19	10	960,5	20	720	418	249	1200	226	704
200	89	60	960,5	20	740	418	250	1200	226	704
200	146	86	960,4	20	693	418	252	1200	226	714
200	78	44	960,4	20	684	418	250	1200	226	724
200	41	0	960,3	20	767	418	261	1200	226	624
200	59	16	960,3	20	766	418	259	1200	226	631
200	61	10	960,3	20	762	418	259	1200	226	641

Table 9: Transfer field scan. 11 k Ω decoupling resistor. Part 2.

time [s]	#1	#2	p [mbar]	T [°C]	H ₂ O [ppm]	U _{GEM2} [V]	U _{GEM1} [V]	Drift [V]	Ind [V]	T [V]
200	35	0	960,6	20	620	420	260	1200	224	624
200	45	5	960,8	20	666	420	259	1200	224	634
200	58	15	960,8	20	660	420	258	1200	224	644
200	72	32	960,8	20	628	420	261	1200	224	654
200	76	46	960,8	20	605	420	259	1200	224	664
200	110	66	961	20	597	420	259	1200	224	674
200	202	128	961	20	638	420	259	1200	224	684
200	77	48	961,2	20	650	418	258	1200	226	694
200	33	22	961,3	20	594	418	258	1200	226	704
200	158	87	961,3	20	648	418	259	1200	226	714
200	129	75	961,4	20	627	418	256	1200	226	724
200	58	15	965,6	20	224	420	260	1200	224	649
200	80	39	966	20	228	420	259	1200	224	659
200	72	40	966	20	224	419	259	1200	225	669
200	98	55	966,1	20	231	419	258	1200	225	679
200	42	22	966,1	20	227	418	258	1200	226	689
200	64	47	967,7	20	232	419	258	1200	225	664
200	89	68	967,7	20	232	419	258	1200	225	674
200	74	55	967,8	20	227	419	257	1200	225	684
200	86	69	967,9	20	225	419	257	1200	225	694
200	204	181	967,9	20	215	419	257	1200	225	704
200	133	120	968	20	238	419	254	1200	225	714
200	55	29	968	20	222	419	258	1200	225	654
200	41	7	968	20	237	419	258	1200	225	644
200	37	0	968,1	20	224	419	258	1200	225	634

Table 10: Induction field scan. 11 k Ω decoupling resistor.

time [s]	#1	#2	p [mbar]	T [°C]	H ₂ O [ppm]	U _{GEM2} [V]	U _{GEM1} [V]	Drift [V]	Ind [V]	T [V]
200	120	8	977,6	20	236	440	259	1200	1309	76
200	61	8	977,7	20	229	440	249	1200	1320	75
200	68	21	977,7	20	233	439	246	1200	1330	77
200	61	37	977,7	20	235	441	235	1200	1339	76
200	45	37	977,9	20	225	440	235	1200	1350	76
200	61	56	977,9	20	234	440	235	1200	1360	75
200	38	37	977,7	20	243	440	236	1200	1370	75
200	46	46	977,7	20	232	440	232	1200	1380	76
200	112	3	977,6	20	237	440	257	1200	1300	79
200	112	2	977,6	20	229	440	254	1200	1289	81
200	98	0	977,6	20	232	440	254	1200	1280	79
200	111	0	977,6	20	223	439	254	1200	1270	80

Table 11: Transfer field scan. 51 k Ω decoupling resistor.

time [s]	#1	#2	p [mbar]	T [°C]	H ₂ O [ppm]	U _{GEM2} [V]	U _{GEM1} [V]	Drift [V]	Ind [V]	T [V]
200	43	1	978,3	20	230	421	259	1200	225	778
200	48	3	978,3	20	226	421	259	1200	225	788
200	47	7	978,4	20	250	421	259	1200	225	798
200	48	23	978,4	20	248	421	259	1200	225	808
200	45	28	978,5	20	242	421	259	1200	225	818
200	52	37	978,6	20	245	421	260	1200	225	828
200	38	27	978,6	20	226	421	258	1200	225	838
200	15	11	978,6	20	255	421	258	1200	225	848
200	59	47	978,8	20	244	421	261	1200	225	857
200	53	43	978,9	20	246	421	259	1200	225	868
200	55	45	978,9	20	235	421	259	1200	225	878
200	76	61	978,9	20	252	421	259	1200	225	888
200	68	45	978,9	20	246	421	259	1200	225	898
200	25	1	972,8	20	223	421	259	1200	225	778
200	33	3	972,7	20	225	421	259	1200	225	788
200	35	5	972,7	20	229	421	259	1200	225	798
200	43	11	972,5	20	222	421	259	1200	225	808
200	47	23	972,5	20	235	421	259	1200	225	818
200	35	19	972,5	20	212	421	260	1200	225	827
200	40	31	972,5	20	243	421	260	1200	225	837
200	44	39	972,4	20	220	421	260	1200	225	847
200	62	55	972,3	20	228	421	260	1200	225	858
200	68	62	972,3	20	235	421	259	1200	225	868
200	56	50	972,3	20	218	421	259	1200	225	878
200	77	75	972,3	20	236	421	259	1200	225	888

Table 12: Induction field scan. 51 k Ω decoupling resistor.

time [s]	#1	#2	p [mbar]	T [°C]	H ₂ O [ppm]	U _{GEM2} [V]	U _{GEM1} [V]	Drift [V]	Ind [V]	T [V]
200	21	2	968	20	220	425	263	1200	1410	144
200	25	3	968	20	219	426	262	1200	1419	145
200	21	7	968	20	216	425	263	1200	1430	144
200	39	23	968	20	215	425	262	1200	1440	145
200	33	22	968	20	218	424	262	1200	1450	146
200	36	31	968	20	220	425	263	1200	1459	145
200	44	41	968	20	218	424	262	1200	1470	146
200	40	38	968	20	219	425	263	1200	1480	144

Table 13: Transfer field scan. 100 k Ω decoupling resistor.

time [s]	#1	#2	p [mbar]	T [°C]	H ₂ O [ppm]	U _{GEM2} [V]	U _{GEM1} [V]	Drift [V]	Ind [V]	T [V]
200	46	2	965,6	20	221	419	261	1200	225	915
200	37	1	965,5	20	238	419	260	1200	225	925
200	25	1	965,5	21	241	419	261	1200	225	935
200	31	4	965,3	21	226	419	260	1200	225	945
200	30	6	965,3	21	233	419	259	1200	225	956
200	36	10	965,3	21	237	419	261	1200	225	965
200	23	11	965,3	21	237	419	260	1200	225	975
200	33	18	965,3	21	227	419	260	1200	225	985
200	37	17	965,3	21	235	419	260	1200	225	995
200	33	19	965,2	21	232	419	262	1200	225	1004
200	32	25	965,2	21	238	419	261	1200	225	1015
200	26	24	964,9	21	236	419	261	1200	225	1025
200	31	26	965	21	234	419	261	1200	225	1035
200	27	23	965	21	227	419	259	1200	225	1046
200	34	33	965	21	230	419	261	1200	225	1055

Table 14: Induction field scan. 100 k Ω decoupling resistor.

time [s]	#1	#2	p [mbar]	T [°C]	H ₂ O [ppm]	U _{GEM2} [V]	U _{GEM1} [V]	Drift [V]	Ind [V]	T [V]
400	20	8	958,7	20	210,9	425	262	1200	1500	145
400	51	1	958,7	20	221	425	263	1200	1480	144
400	61	37	958,8	20	218	425	262	1200	1520	145
400	83	66	958,8	20	222	425	262	1200	1540	145
400	84	76	959	20	228	425	263	1200	1560	144
400	113	111	960	20	233	424	263	1200	1581	144
400	63	62	959	21	232	425	262	1200	1600	145
400	9	0	959	20	232	425	203	1200	1460	144
400	36	2	959	20	230	425	263	1200	1460	144

Table 15: Transfer field scan. New GEM1. Discharges in GEM2. First Scan.

time [s]	#1	#2	p [mbar]	T [°C]	H ₂ O [ppm]	U _{GEM2} [V]	U _{GEM1} [V]	Drift [V]	Ind [V]	T [V]
200	16	2	964,7	20	143	416	259	1200	227	535
200	19	2	964,8	20	146	416	259	1200	227	545
200	18	2	964,8	20	137	416	258	1200	227	555
200	19	2	964,8	20	147	416	259	1200	227	565
200	39	6	964,7	20	134	416	258	1200	227	575
200	24	4	964,7	20	138	416	257	1200	227	585
200	36	2	964,7	20	133	416	257	1200	227	595
200	33	2	964,7	20	138	416	257	1200	227	605
200	36	10	964,7	20	132	416	257	1200	227	615
200	43	9	964,7	20	129	416	257	1200	227	626
200	23	5	964,8	20	138	416	257	1200	227	635
200	27	4	964,8	20	130	416	257	1200	227	646
200	38	14	964,8	20	135	416	258	1200	227	655
200	29	5	964,8	20	128	416	258	1200	227	665
200	33	14	964,8	20	133	416	257	1200	227	676
200	36	14	964,8	20	130	416	258	1200	227	685
200	42	23	965	20	124	416	257	1200	227	696
200	46	22	965	20	137	416	257	1200	227	705
200	58	37	965	20	122	416	257	1200	227	716
200	55	47	965	20	128	416	257	1200	227	725
200	37	35	965	20	130	416	253	1200	227	736
200	25	25	965	20	129	416	251	1200	227	746
200	26	25	965	21	126	416	253	1200	227	755
200	34	34	965	21	127	416	252	1200	227	766

Table 16: Transfer field scan. New GEM1. Discharges in GEM2. Second scan.

time [s]	#1	#2	p [mbar]	T [°C]	H ₂ O [ppm]	U _{GEM2} [V]	U _{GEM1} [V]	Drift [V]	Ind [V]	T [V]
400	40	2	974,9	19	106	419	263	1200	226	523
400	63	11	974,9	19	106	419	263	1200	226	533
400	57	12	974,9	20	103	419	263	1200	226	543
400	69	22	974,9	20	105	419	262	1200	226	553
400	76	17	974,9	20	98	419	263	1200	226	563
400	86	24	975	20	98	419	262	1200	226	573
400	75	16	974,9	20	100	419	263	1200	226	583
400	108	32	974,9	20	98	419	264	1200	226	592
400	79	29	975,1	20	92	419	262	1200	226	604
400	97	45	975	20	96	419	263	1200	226	613
400	79	32	975,2	20	97	419	263	1200	226	623
400	85	38	975,2	20	99	419	263	1200	226	633
400	107	56	975,3	20	96	419	263	1200	226	643
400	78	38	975,4	20	97	419	263	1200	226	653
400	78	51	975,4	20	95	419	263	1200	226	663
400	87	52	975,4	20	97	419	262	1200	226	674
400	96	64	975,5	20	95	419	263	1200	226	683
400	81	50	975,5	20	97	419	263	1200	226	693
400	98	69	975,5	20	94	419	262	1200	226	704
300	84	67	975,6	20	95	419	262	1200	226	714
300	74	60	975,7	20	94	419	263	1200	226	723
300	112	99	975,8	20	90	419	262	1200	226	734
300	37	35	975,8	20	92	419	260	1200	226	744
300	65	61	975,8	20	91	419	261	1200	226	753
300	71	71	975,9	20	94	419	261	1200	226	763

Table 17: Induction field scan. New GEM1. Discharges in GEM2.

time [s]	#1	#2	p [mbar]	T [°C]	H ₂ O [ppm]	U _{GEM2} [V]	U _{GEM1} [V]	Drift [V]	Ind [V]	T [V]
200	24	2	966,6	20	113	430	257	1200	1249	101
200	25	3	966,7	20	115	429	257	1200	1260	100
200	19	8	966,7	20	115	430	256	1200	1270	99
200	21	12	966,8	20	116	429	257	1200	1280	100
200	36	32	966,9	20	110	431	257	1200	1289	99
200	35	33	966,9	20	114	430	256	1200	1299	101
200	31	30	967	20	114	431	257	1200	1309	99
200	25	25	967	20	112	430	256	1200	1320	100
200	29	29	967	20	114	430	257	1200	1330	99
200	27	2	967	20	113	430	258	1200	1240	99
200	22	0	967,1	20	114	429	257	1200	1230	100
200	25	0	967,3	20	114	431	257	1200	1219	99

Table 18: Transfer field scan. Discharges in GEM1. Part 1

time [s]	#1	#2	p [mbar]	T [°C]	H ₂ O [ppm]	U _{GEM2} [V]	U _{GEM1} [V]	Drift [V]	Ind [V]	T [V]
600	64	64	976,7	20	98	99	429	1200	198	1101
600	70	69	976,7	20	101	250	430	1200	198	1101
600	96	96	976,8	20	98	250	431	1200	198	1090
600	87	85	976,9	20	98	250	430	1200	198	1081
600	87	87	977	20	94	250	430	1200	198	1071
600	84	83	977,1	20	100	250	429	1200	198	1061
600	84	81	977,1	20	103	250	429	1200	198	1021
600	79	75	977,3	20	95	250	429	1200	198	1011
600	79	77	977,4	20	98	250	429	1200	198	991
600	60	50	977,5	20	96	250	429	1200	198	951
600	59	51	977,6	20	98	250	430	1200	198	970
600	73	67	977,8	20	97	250	429	1200	198	961
600	78	70	977,8	20	95	250	430	1200	198	941
600	68	61	977,9	20	98	250	429	1200	198	931
600	93	81	977,8	20	97	250	430	1200	198	921
600	77	69	978	20	94	250	429	1200	198	911
600	95	81	978,1	20	97	250	429	1200	198	891
600	39	11	983,3	20	118	250	429	1200	198	790
600	40	8	983,5	20	116	250	428	1200	198	801
600	49	17	983,4	20	110	250	429	1200	198	810
600	46	20	983,1	20	104	250	428	1200	198	821
600	40	22	982,3	20	93	250	429	1200	198	830
600	38	22	982,3	20	95	250	430	1200	198	840
600	52	41	982,2	20	95	250	429	1200	198	850
600	45	33	982,1	20	93	250	429	1200	198	860

Table 19: Transfer field scan. Discharges in GEM1. Part 2

time [s]	#1	#2	p [mbar]	T [°C]	H ₂ O [ppm]	U _{GEM2} [V]	U _{GEM1} [V]	Drift [V]	Ind [V]	T [V]
600	48	41	982	20	94	250	428	1200	198	871
600	49	45	982	20	96	250	429	1200	198	880
600	47	8	981,5	20	94	250	429	1200	198	780
600	57	8	981,3	20	92	250	429	1200	198	770
600	47	6	981,1	20	91	250	429	1200	198	760
600	61	2	981,1	20	88	250	429	1200	198	750
600	48	2	981	20	91	250	429	1200	198	740
600	62	1	980,8	20	93	250	429	1200	198	730
600	34	1	980,8	20	90	250	429	1200	198	720
600	37	0	980,8	20	91	250	429	1200	198	710
600	63	0	980,7	20	87	250	429	1200	198	700
600	67	0	980,7	20	91	250	429	1200	198	690

List of Figures

1.	ALICE	3
2.	ALICE TPC	6
3.	Gating Grid	7
4.	TPC Performance	8
5.	ALICE Setup	9
6.	Simulation of electric field	10
7.	Stack of four GEMs	11
8.	IROC GEM	12
9.	Potentials of a GEM during a discharge.	14
10.	Potentials of a GEM during a secondary discharge.	15
11.	Picture of the setup.	18
12.	Schematic of the setup.	18
13.	Schematic of HV probe position at GEM top side.	20
14.	Counting logic that distinguishes between primary and secondary signal according to the amplitude height	22
15.	Counting logic that distinguishes between primary and secondary signal according to the time difference	22
16.	Comparison of secondary discharge probability of two different foils as GEM2. Discharges were triggered in GEM2. The detailed settings for the measurements can be found in Appendix A in Tab. 6 and Tab. 5.	25
17.	The secondary probability for different foils in the location of GEM1, the discharges were triggered in GEM2.	26
18.	Position of decoupling resistor at the GEM bottom HV supply path.	28
19.	Transfer field scan for different decoupling resistors.	29
20.	Induction field scan for different decoupling resistors.	29
21.	Electric field (over pressure) for which the secondary probability is 50% as a function of the resistor value.	31
22.	Measurements with a one GEM detector executed in Munich	32
23.	Signal from readoutplane depicting different heights of primary and secondary amplitude for a setup without decoupling resistor.	33
24.	Signal from readoutplane depicting same heights of primary and secondary amplitude for a setup with 51 k Ω decoupling resistor.	33

25.	Time difference between primary and secondary discharges in dependence of the electric field over the pressure. Setup with no decoupling resistor. Transfer field scan with discharges triggered in GEM2.	35
26.	Time difference between primary and secondary discharges in dependence of the electric field over the pressure. Setup with 11 k Ω . Transfer field scan with discharges triggered in GEM2.	35
27.	GEM1 potentials during a primary and secondary discharge.	37
28.	GEM2 potentials during a primary and secondary discharge.	38
29.	GEM potentials for discharge in transfer field.	39
30.	GEM potentials for discharge in induction field.	39
31.	Probability of potential change in a setup with no decoupling resistor. . .	41
32.	Propagation probability in a setup with no decoupling resistor.	41
33.	Probability of potential change in a setup with 11 k Ω decoupling resistor.	42
34.	Propagation probability in a setup with 11 k Ω decoupling resistor.	42
35.	Discharges triggered in GEM1 compared to discharges triggered in GEM2 for a transfer field scan. The detailed settings can be found in Appendix A Tab. 15, Tab. 16, Tab. 18 and Tab. 19	44
36.	Potentials of GEM2 during discharges triggered in GEM1. Setup with no decoupling resistor. Transfer field scan.	45
37.	Potentials of GEM2 during discharges triggered in GEM1. Setup with no decoupling resistor. Transfer field scan.	45

References

- [1] *CERN Homepage*. <https://home.cern/about> [Rev. 3.03.2017].
- [2] *The Nobel Prize in Physics 1992*. http://www.nobelprize.org/nobel_prizes/physics/laureates/1992/charpak-facts.html [Rev. 3.03.2017].
- [3] A. Andronic. "An overview of the experimental study of quark-gluon matter in high-energy nucleus-nucleus collisions". 2014, arXiv:1407.5003v1 [nucl-ex].
- [4] *ALICE- Allgemeines*. <http://www.lhc-facts.ch/index.php?page=alice> [Rev. 3.03.2017].
- [5] The ALICE Collaboration. "The ALICE Experiment at the CERN LHC". In: *J. Inst.* 3 (2008), S08002.
- [6] S. Masciocchi. "Presentation: The ALICE Detector". In: *Lecture: Recent Results from the LHC*. Ruprecht-Karls-Universität Heidelberg, May 2, 2014. http://results-lhc.physi.uni-heidelberg.de/Lectures/ALICE/sma_LHC_ALICE_1.pdf [Rev. 2.03.2017].
- [7] Private communication with S. Masciocchi.
- [8] J. Alme et al. "The ALICE TPC, a large 3-dimensional tracking device with fast readout for ultra-high multiplicity events". In: *Nucl. Instrum. Methods Phys. Res., A* 622 (2010), pp. 316–367.
- [9] *The ALICE Experiment*. http://aliceinfo.cern.ch/Public/en/Chapter2/Chap2_TPC.html [Rev. 27.2.2017].
- [10] The ALICE Collaboration. *Upgrade of the ALICE Time Projection Chamber*. Technical Design Report, CERN-LHCC-2013-020, ALICE-TDR-016. 2014.
- [11] H. Appelshäuser. *Presentation: ALICE TPC Upgrade Progress Report*. April 5, 2016. <https://indico.cern.ch/event/509380/contributions/2031104/attachments/1253026/1848445/AW-HA-Apr-5-2016.pdf> [Rev. 2.03.2017].
- [12] *Gas Amplification in Micro Pattern Detectors* <https://www.lctpc.org/e8/e46/> [Rev. 2.03.2017].
- [13] S. Masciocchi. "Presentation: Gaseous Detectors." In: *Lecture: Physics of Particle Detectors*. Ruprecht-Karls-Universität Heidelberg, May, 2016.

- [14] H. Kolanoski, N. Wermes. *Teilchendetektoren. Grundlagen und Anwendungen*. Berlin, Heidelberg: Springer, 2016.
- [15] The ALICE Collaboration. "Performance of the ALICE experiment at the CERN LHC". In: *International Journal of Modern Physics A*, Vol. 29, No. 24 (2014).
- [16] B. Abelev. "Upgrade of the ALICE Experiment: Letter Of Intent". In: *Journal of Physics G: Nuclear and Particle Physics*, Vol. 41, No. 8 (2014).
- [17] F. Sauli. "GEM: A new concept for electron amplification in gas detectors". In: *Nucl. Instrum. Methods Phys. Res., A* 386 (1997), pp. 531–534.
- [18] M. Beger et al. "A Large Ungated TPC with GEM Amplification". Preprint for: *Nucl. Instrum. Methods Phys. Res.*, February 20, 2017.
- [19] S. Pinto et al. "Progress on large area GEMs". In: *J. Inst.* A 4 (2009).
- [20] F. Sauli. "The gas electron multiplier (GEM): Operating principles and applications". In: *Nucl. Instrum. Methods Phys. Res., A* 805 (2016), pp. 2–24.
- [21] F. V. Böhmer et al. "Simulation of space charge effects in an ungated GEM-based TPC". In: *Nucl. Instrum. Methods Phys. Res., A* 719 (2013), pp. 101–108.
- [22] S. Bachmann et al. "Discharge studies and prevention in the gas electron multiplier." In: *Nucl. Instrum. Methods Phys. Res., A* 479 (2002), pp. 294–308.
- [23] A. Deisting, P. Gasik. *Presentation: Discharge and stability studies for the read-out chambers of the upgraded ALICE TPC*. INSTR17, March 2, 2017. <https://aliceinfo.cern.ch/node/28350> [Rev. 10.3.17].
- [24] V. Peskov, P. Fonte. "Research on discharges in micropattern and small gap gaseous detectors". In: *ArXiv e-prints*. (2009). arXiv:0911.0463v1 [physics.ins-det].
- [25] P. Gasik, A. Deisting "Presentation: Discharge studies with single GEMs". June 7, 2016.
- [26] P. Gasik. *Presentation: Single GEM Discharge Studies with a nominal HV scheme*, TU München, September 13, 2016.
- [27] A. Deisting, C. Garabatos, A. Szabo, D. Vranic. "Measurements of ion mobility in argon and neon based gas mixtures". In: *Nucl. Instrum. Methods Phys. Res., A* 845 (2017), pp. 215–217.

- [28] A. Deisting, A. Szabo. *Presentation: Double GEM studies of secondary discharges*. TPC Upgrade Meeting, September 20, 2016. <https://indico.cern.ch/event/407312/contributions/2309244/> [Rev. 10.3.17].
- [29] P. Gasik. "Discharge studies with single- and multi-GEM structures in a scope of the ALICE TPC upgrade". RD51 Meeting, February, 2016. https://indico.cern.ch/event/496113/contributions/2008281/attachments/1242032/1827187/gasik_11032016_sparks_RD51.pdf
- [30] D. Miskowiec. TPC Upgrade Meeting at GSI. January 16, 2017.
- [31] S. Masciocci. "Presentation: The ALICE upgrade program". In: *EMMI NQM seminar*. GSI Darmstadt, November 16, 2016. http://web-docs.gsi.de/~andronic/emmi_nqm_seminar/2016/sma_ALICEupgrade.pdf [Rev. 2.03.2017].
- [32] W. Blum et al. *Particle Detection with Drift Chambers*. Berlin, Heidelberg: Springer, 2008.

Erklärung

Ich versichere, dass ich diese Arbeit selbstständig verfasst und keine anderen als die angegebenen Quellen und Hilfsmittel benutzt habe.

Heidelberg, den 13.03.2017